Precambrian Research 233 (2013) 316–336

Contents lists available at SciVerse ScienceDirect

Precambrian Research

journal homepage: www.elsevier.com/locate/precamres

Meso/Neoarchean crustal domains along the north Konkan coast, western India: The Western Dharwar Craton and the Antongil-Masora Block (NE Madagascar) connection

S. Rekha [a,*], T.A. Viswanath [b], A. Bhattacharya [a], N. Prabhakar [a]

[a] Department of Geology and Geophysics, Indian Institute of Technology, Kharagpur 721302, India
[b] Department of Earth Sciences, Goa University, Taleigao Plateau, Goa 403206, India

ARTICLE INFO

Article history:
Received 16 December 2012
Received in revised form 7 May 2013
Accepted 21 May 2013
Available online 31 May 2013

Keywords:
Antongil-Masora Block (Madagascar)
Western Dharwar Craton (India)
Monazite chemical ages
Mesoarchean
Neoarchean
Gondwanaland

ABSTRACT

Synthesis of mesoscopic structures and microscopic analyses of fabric superposition and deformation microstructures are combined with Th–U–Pb (total) ages in monazites to constrain the Meso/Neoarchean crustal domains in the Western Dharwar Craton (WDC) along the western coast of India; the domains are correlated with those in NE Madagascar to configure the assembly of crustal domains in the East Gondwanaland prior to the Mesozoic break up. In the WDC, para-schists and phyllites of the Shimoga schist belt, SSB (unmixed age components, 3067 ± 26 and 3158 ± 110 Ma) and the Peninsular gneisses (3138 ± 35 Ma) are intruded by granitoid plutons (2924 ± 50 Ma) deformed at low-T. Five generations of deformation events are identified in the SSB and Peninsular gneisses. But the two early tectonic fabrics in Peninsular gneisses formed at anatectic amphibolite facies conditions are in sharp contrast to fabrics in SSB formed at greenschist facies. The two lithodemic units are inferred to share a pre-3.2 Ga tectonic contact.

By contrast, in the Goa schist belt (GSB), phyllites/schists (unmixed ages – 2436 ± 34, 2543 ± 66 and 2625 ± 36 Ma) and polymict conglomerates (unmixed ages – 2458 ± 34 and 2566 ± 53 Ma) possess two generations of tectonic fabrics and are the youngest dated metamorphic unit in the WDC. The deformed Quepem granitoid pluton located along the axial zone of the regional-scale N-trending gently plunging upright folds in GSB yields comparable chemical age (2565 ± 33 Ma). Angular to sub-rounded and boulder to granule sized polymict clasts of Peninsular gneisses (3128 ± 60 Ma), foliated granitoids, amphibolites, BIFs and low-grade quartzite/chlorite-muscovite schists in GSB para-conglomerates suggest the sediments deposited in shallow basin were derived from neighboring sources, e.g. the Peninsular gneisses and SSB supracrustals. The Neoarchean deformation-metamorphism marks the closure of the Goa basin synchronous with the 2.4–2.6 Ga accretion of the West and the East Dharwar Cratons.

Based on the results of this study, the following correlation among Mesoarchean–Neoarchean crystallites in the Western Dharwar Craton and the Antongil-Masora Block, NE Madagascar (*in italics below*) appears realistic, e.g. 2.4–2.6 Ga Goa schist belt ≈ *Mananara Group*; 2.5 Ga Quepem granitoid ≈ *Masoala Suite*; 3.1 Ga Shimoga schist belt ≈ *Fenerivo Group*; 3.1 Ga Peninsular gneiss suite ≈ *Nosy Boraha suite*.

1. Introduction

The Earth's history is marked by episodic agglomeration and dispersal of the continental lithosphere (Gurnis, 1988; Wilson, 1966). Re-assembling supercontinents from their dispersed fragments involves retrieval of the pre-drift configuration of rifted crustal fragments and comparing their crustal evolutionary histories (Payne et al., 2009). Tracing regional shear/thrust zones across rifted continental landmasses is important to link continental fragments (Fitzsimons, 2000; Katz and Premoli, 1979; Sacks et al., 1997; Shackleton, 1996; Stern, 1994; Windley et al., 1994). The present landmass of Madagascar, located at the margin of East and West Gondwana land (Fig. 1), comprises fragments of Archean crustal domains of Africa and India amalgamated during the Late Neoproterozoic (720–620 Ma; Blasband et al., 2000; Stern, 1994) and the Early Paleozoic (570–520 Ma; Collins and Pisarevsky, 2005; Kröner et al., 2000; McWilliams, 1981; Meert et al., 1995; Unrug, 1996; Veevers, 2004) assembly of the Gondwana Supercontinent (Borg and De Paolo, 1991; Cayley, 2011; Collins and Pisarevsky, 2005; Dalziel, 1991; Hoffman, 1991; Kusky and Matsah, 2003; Moores, 1991; Rogers and Santosh, 2003; Torsvik et al., 1996; Trompette, 2000; Tucker et al., 1999, 2011a; Weil et al., 1998).

* Corresponding author. Tel.: +91 9647182768.
E-mail addresses: rekha.eas@yahoo.com, georekha@gmail.com (S. Rekha).

0301-9268/$ – see front matter © 2013 Elsevier B.V. All rights reserved.
http://dx.doi.org/10.1016/j.precamres.2013.05.008

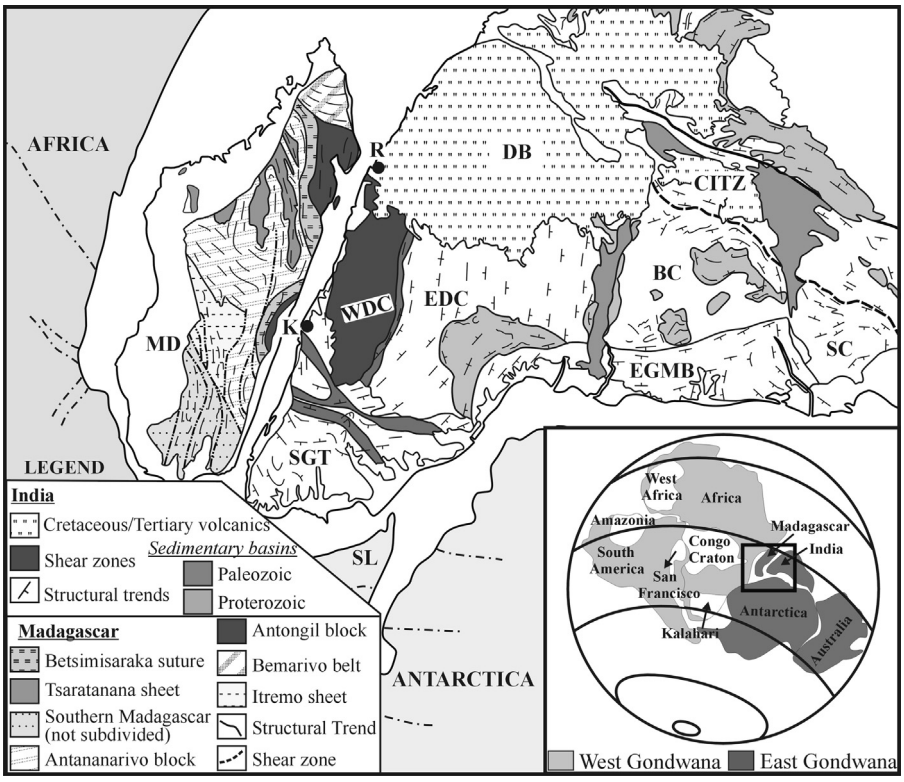

Fig. 1. Paleoposition of Madagascar and India as part of East Gondwana (modified after Yoshida and Santosh, 1996) at 500 Ma. Inset shows pre-drift Gondwanaland configuration (after Sommer et al., 2003). Major tectonic divisions of Madagascar (after Collins et al., 2003), and India (modified after Narayanaswami, 1966) are shown. Precambrian crystalline terranes in India (in white) along with major structural trends are shown. The identity of the Betsimisaraka suture is contested by Tucker et al. (2011a). The Western Dharwar Craton (India) and the Antongil-Masora Block (Madagascar) are highlighted in dark gray shade. MD = Madagascar, SL = Sri Lanka, WDC = Western Dharwar Craton, EDC = Eastern Dharwar Craton, SGT = Southern Granulite Terrain, EGMB = Eastern Ghats Mobile Belt, SC = Singhbhum Craton, BC = Bastar Craton, DB = Deccan Basalt, CITZ = Central Indian Tectonic Zone. The Konkan coast extends from Kasargod (K) in south to Ratnagiri (R) in the north.

Paleogeographic reconstructions based on paleomagnetic and geological data suggest that Madagascar was demonstrably contiguous with India at 530 Ma (Collins and Pisarevsky, 2005; De Wit, 2003; Lawver and Scotese, 1987; Fig. 1). Tucker et al. (1999, 2011a) suggested the Antongil Block, the oldest known crustal domain in NE Madagascar, shared a coherent Paleo/Mesoarchean evolutionary history with the Western Dharwar Craton (WDC) of India (Fig. 1). The authors point to the broad overlap in U–Pb zircon age (3187 ± 2 Ma) and Sm–Nd Model age (3204 Ma) obtained from migmatitic orthogneisses at Ile Sainte Marie in the Antongil Block, and Rb–Sr and Pb–Pb ages available from Peninsular gneisses from the WDC in India (3.4–3.0 Ga; Beckinsale et al., 1980; Bhaskar Rao et al., 1991; Meen et al., 1992; Peucat et al., 1995; Taylor et al., 1984). According to Tucker et al. (1999, 2011a) the broad overlap in εNd and εSr values (2500 Ma) between the "Dharwar gneisses and anatectic granites" and similar rocks from Ile Sainte Marie and Alaotra-Beforona areas in Madagascar support the once contiguous nature of the Antongil Block and the WDC. Recent U–Pb SHRIMP ages (3.1–3.3 Ga) in three samples from the Nosy Boraha suite determined by Tucker et al. (2011a) re-emphasizes that these ancient rocks were broadly coeval with the Peninsular gneisses in the Western Dharwar Craton.

In recent years, in areas neighboring the NE coast of Madagascar, new geological (Pili et al., 1997; Raharimahefa and Kusky, 2006, 2010; Tucker et al., 2011a,b), petrological (Buchwaldt et al., 2003; Jöns et al., 2009) and chronological (Paquette et al., 2003; Schofield et al., 2010; Thomas et al., 2009) data have helped to identify different lithodemic units and shear/thrust zones separating these units (Fig. 1). The continuity of "equivalent" rocks eastwards into western India is unknown due to the lack of geological, petrological and chronological data along the western coast of India. Except Rb–Sr ages obtained from areas neighboring Goa (Dhoundial et al., 1987), available structural, petrological and chronological information from the WDC are located 50–100 km inwards from the western coast of India (Figs. 2 and 3). This lack of critical geologic information along the northern Konkan coast impedes a comprehensive space-time correlation of lithodemic units along the north-eastern coast of Madagascar with those in the Konkan coast (India) that arguably represent the rifted margin of the landmasses of Madagascar and India shared prior to the break up of Gondwanaland in the Late Cretaceous.

In this study, we provide structural settings, petrological characteristics and U–Pb–Th chemical ages of texturally constrained monazites in a wide variety of Precambrian lithologic units along the northern parts of the Konkan coast. The information is compiled with lithologic-structural data to evaluate the common tectonic histories between NE Madagascar and western India in the Archean time.

2. Geological outline of WDC from inland areas: previous studies

The Western Dharwar Craton (WDC) comprises several lithodemic units, the most expansive among these are the Peninsular gneisses and the N/NNW-trending supracrustal belts (Fig. 2). The Peninsular gneisses comprise tonalite-trondhjemite-granodiorite polyphase migmatite gneisses and the homophanus trondhjemite-granodiorite plutons of Paleo/Mesoarchean in age (>3.0 Ga; Fig. 3). The Gorur gneiss (~3.4 Ga; Beckinsale et al., 1980) and the Anmod Ghat trondhjemite gneiss (~3.4 Ga; Dhoundial et al., 1987) are the oldest dated rocks in the WDC, and are considered to be the basement rocks in the craton. The supracrustal belts are sub-divided

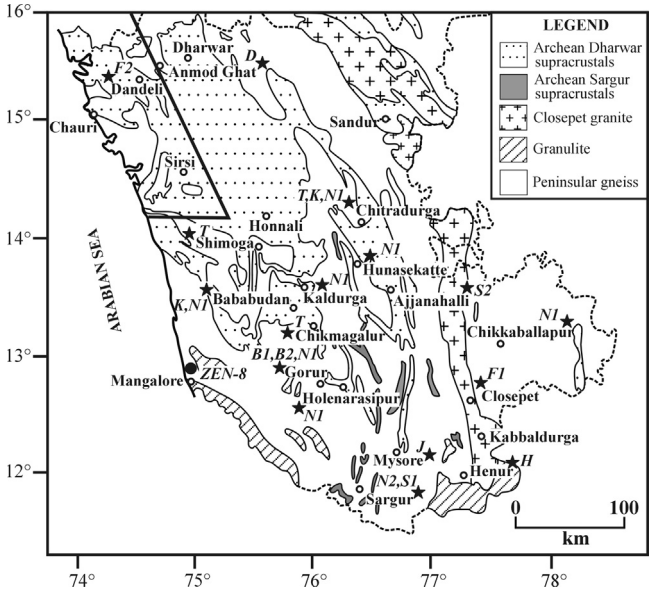

Fig. 2. Generalized geological map of the Western Dharwar Craton (modified after Naha et al., 1991). The study area along the west coast of India shown by thick continuous line (Chauri is indicated). Localities mentioned in the text are shown with open circles. Location of sample ZEN-8, used for monazite dating is shown with filled circle (locations of other monazite dated samples are shown in Fig. 4). Filled-stars are generalized locations of published ages from the WDC (for details of ages refer to Fig. 3): B1 = Bhaskar Rao et al. (1991); B2 = Beckinsale et al. (1980); D = Dhoundial et al. (1987); F1 = Friend and Nutman (1991); F2 = French and Heaman (2010); F3 = French et al. (2004); H1 = Halls et al. (2007); H2 = Hokada et al. (2012); J = Jayananda et al. (2008); K = Kumar et al. (1996); M = Maya et al. (2011); N1 = Naha et al. (1993); N2 = Nutman et al. (1992); S1 = Sarangi et al. (2007); S2 = Sarma et al. (2011); T = Taylor et al. (1984).

into the amphibolite facies (granulite facies in southern parts of the WDC) Paleo/Mesoarchean Sargur Group (3.1–3.3 Ga) and the low-grade (dominantly greenschist facies) Neoarchean Dharwar Supergroup (2.6–2.8 Ga) (Ramakrishnan and Vaidyanadhan, 2008). The Dharwar Supergroup (2.6–2.8 Ga) is further classified into the older Bababudan Group and the younger Chitradurga Group separated by a disconformity (Swami Nath and Ramakrishnan, 1981). The older Bababudan Group dominated by meta-basalt/gabbro, ultramafic schist, layered mafic complex, felsic volcanic, siliceous phyllite, cross-bedded quartzite and minor banded iron formation, is lithologically distinct from the Chitradurga Group comprising meta-volcanic, banded iron formation (often Mn-bearing), orthoquartzite, meta-carbonate, greywacke, polymict conglomerate horizon, and siliceous phyllite. Three episodes of regional scale

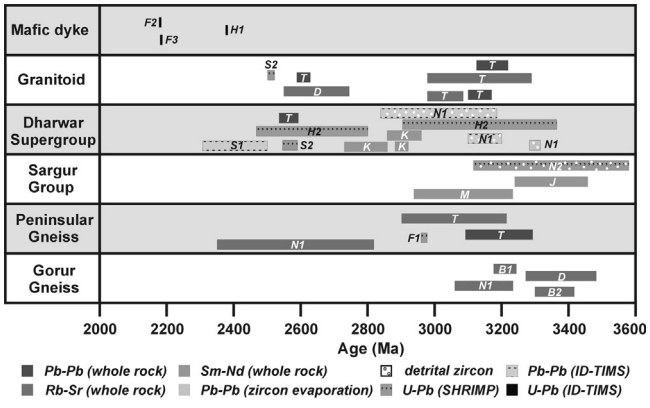

Fig. 3. Summary of published ages of lithological units in the WDC. Refer to Fig. 2 for list of acronyms.

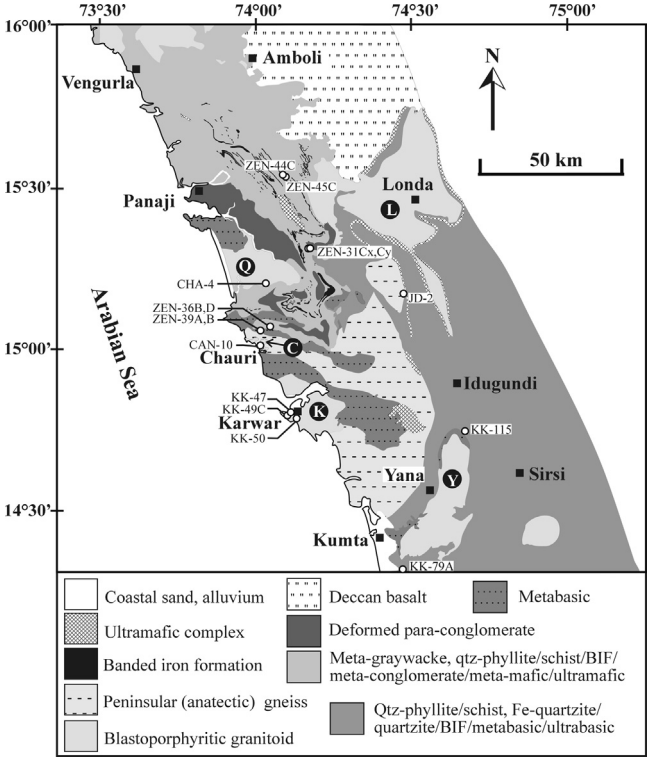

Fig. 4. Simplified lithological map of the northern Konkan coast compiled from geological maps of the state of Goa, Sindhudurg district (Maharashtra), and the state of Karnataka published by the Geological Survey of India (1996, 1995 and 1981). Locations of monazite-dated samples from this study (open circles) and key localities (filled rectangles) referred in the text are shown. L, Q, C, K and Y are acronyms for granitoid plutons in around Londa, Quepem, Chauri, Karwar and Yana respectively. The State of Goa encompasses the area south of Vengurla, north of Karwar, west of Londa, and SW of Amboli.

folding events are recognized in the supracrustal belts and the Peninsular gneisses. Isoclinal folds on mineralogical layering in Peninsular gneisses and supracrustals with development of penetrative axial planar foliation marked the first generation folds. These were superimposed by upright asymmetric folds with N- to NNW-trending axial planes and gentle to moderately plunging fold axes. The last folding event is manifested by locally developed open folds with E-W trending axial plane (Naha et al., 1986, 1990, 1991, 1993, 1995; Naha and Chatterjee, 1982; Mukhopadhyay, 1986). Expansive felsic magmatism in the WDC occurred in two stages, 3.0–3.2 Ga and 2.5–2.7 Ga (Fig. 3). Proterozoic mafic dykes in three age clusters (2.4 Ga, 2.0–2.2 Ga and 1.6 Ga) (French and Heaman, 2010; French et al., 2004; Halls et al., 2007; Radhakrishna et al., 2004) mark the last phases of activity in WDC.

3. The structural set up of the northern Konkan coastal plain: this study

A 50–60 km wide and 200 km long corridor along the Konkan coastal plain (Fig. 4) from Amboli (Maharashtra) to Kumta (Karnataka) was structurally mapped (Fig. 5). The rocks are poorly exposed along the coastal plain due to deep chemical weathering, and to the east, among the thickly vegetated hills of the Western Ghats, the rocks are inaccessible except in freshly cut road sections, quarries, and rare monadnocks and inselbergs. The area is dominated by Peninsular gneisses (migmatitic tonalite-trondjhemite-granodiorite gneisses), and greenschist facies phyllites, chlorite-muscovite ± calcite ± biotite schists, chlorite-actinolite ± calcite schists, quartzites, quartz-conglomerates and polymict conglomerates. The para-schists/phyllites occur in two belts, e.g. the

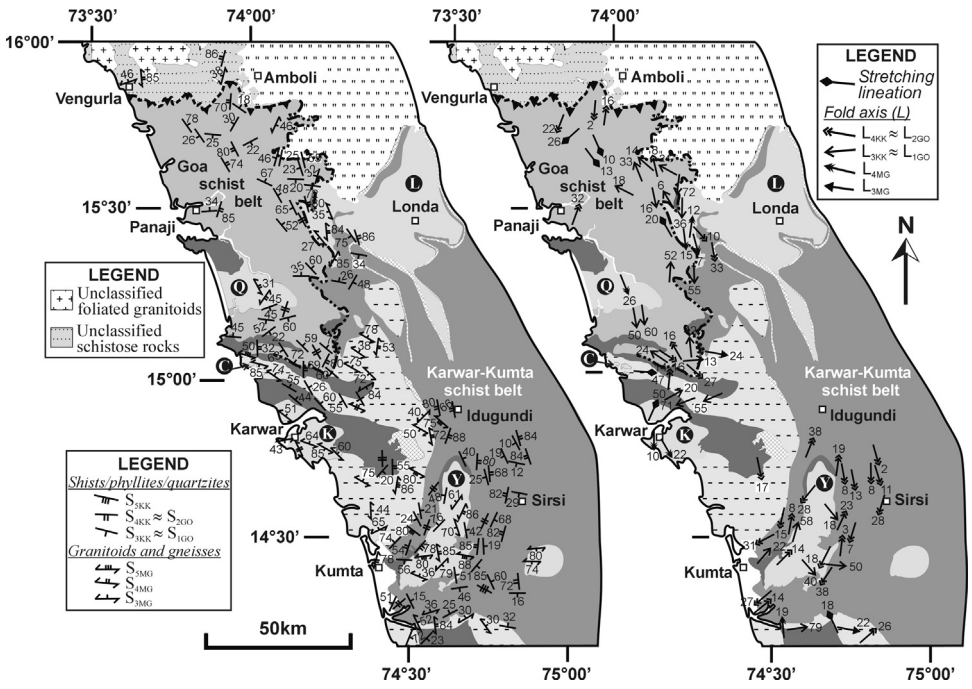

Fig. 5. (a) Planar structures and (b) linear structures along the northern Konkan coast. The legend for lithologic units is same as in Fig. 4, except (a) banded iron formation and ultramafic complex in Goa schist belt in Fig. 4 is omitted, (b) only outlines of deformed para-conglomerate in Fig. 4 is shown, (c) horizontal dots in metabasic units in Fig. 4 are omitted in this figure, and (d) the unclassified schists and granitoids to the North of Vengurla are shown with different symbols in this figure.

Goa schist belt (GSB) in the northern part of the mapped area, and the Karwar-Kumta schists along the strike extension of the NW-trending Shimoga schist belt (SSB) in the east and south (Figs. 4 and 5). Five generations of tectonic fabrics are recognized in the anatectic Peninsular gneisses and in the SSB metasediments. By contrast, para-schists/phyllites and quartzites of the GSB with fewer tectonic fabrics are structurally younger. The gneisses and the supracrustal belts host several blastoporphyritic granitoid plutons around Karwar, Chauri, Londa (tonalite-granodiorite) and Quepem (granodiorite-granite).

3.1. Migmatitic Peninsular gneiss

In Peninsular gneisses, the gneissose structure (Fig. 6a) is defined by the alternation of couple-of-cm to tens-of-cm wide hornblende/biotite-plagioclase dominated melanocratic layers and plagioclase, K-feldspar and quartz dominated leucocratic layers. The layers posses a penetrative tectonic fabric defined by dynamically recrystallized hornblende aggregates anchored to polygonized feldspars in the melanocratic layers (Fig. 6b), and quartz ribbons to which phase/grain margins of polygonized feldspars are pinned in the leucocratic layers (Fig. 6b). Polygonized hornblende sharing triple junction (Fig. 6c) is common in the melanocratic layers. The penetrative foliation is axial planar to intra-layer rootless hinges of isoclinal and eye-shaped folds described by cm-wide leucosome layers (Fig. 6a). The leucosomes, couple of cm wide (herein termed S_{1MG}; MG for migmatite gneiss), and the axial planar foliation (designated S_{2MG}) curve into or are drawn sub-parallel to the gneissic layering (S_{3MG}) in the gneisses (Fig. 6d). In regional scale, the S_{3MG} gneissic fabric is folded with long N/NNW-trending limbs and short E-trending limbs (Fig. 5), but the corresponding axial planar fabric (S_{4MG}) is poorly developed in the area. Greenschist facies epidote-clinozoisite, actinolite and chlorite aggregates replacing the high-T hornblende-plagioclase aggregates defining fabrics (Fig. 6e) possibly correlate with this S_{4MG} deformation event. A set of locally developed E-W closing broad warps and widely spaced E-W trending fracture planes (S_{5MG}) comprise the last deformation event in the rocks. The superposition of structures is similar to that described by Naha et al. (1991, 1995, 1996) in gneissic rocks to the SE of the mapped area.

3.2. The Karwar-Kumta schist belt

The lithodemic unit is dominated by quartzite, ferruginous quartzite, mafic schist and para-schist/phyllite. The early fabrics in para-schists/phyllites are best preserved in an outcrop in the Kudremukh National Park (Fig. 7a and b Lat: N 13° 12.38′: Long: E 75° 11.74′) south of the mapped area in Fig. 5. In this outcrop, the earliest schistosity (S_{1KK}) is crenulated, and the gently dipping crenulation cleavage (S_{2KK}) is warped by the penetrative schistosity, S_{3KK} (Fig. 7a–c; 'KK' is the acronym for the Karwar-Kumta schist belt). The successive fabrics in mafic schists are defined by chlorite-actinolite (Fig. 7d) and rare zoisite; while shape-preferred aggregates of chlorite-muscovite ± biotite define the fabrics in para-schists and phyllites (Fig. 7e). Poles to S_{3KK} fabric in regional scale (Fig. 5) describe a well-defined girdle with the β-axis plunging at low angle (<30°) towards S/SSW and N/NNE consistent with the measured plunges of mesoscopic asymmetric open to close upright F_{4KK} folds with NNW trending axial planes (S_{4KK}) (Fig. 8). The non-plane nature of S_{4KK} and the non-cylindricity of F_{4KK} (Figs. 5 and 8) in regional scale are due to interference by the locally developed younger E-trending cross-folds similar to those observed in migmatitic Peninsular gneisses reported by Naha et al. (1991, 1996).

3.3. The Goa schist belt

Metagreywacke (chlorite-calcite-biotite and chlorite-muscovite ± calcite schist) and inter-banded Banded Iron Formation, quartzite, and chlorite-actinolite bearing amphibolite dominate the schist belt. An intensely deformed horizon of polymict and quartz conglomerates with granule to boulder sized clasts demarcates the southern and the eastern margins of the schist belt (Fig. 9a and b). In the polymict conglomerates, the low-sphericity clasts are Banded Iron Formation, quartzite,

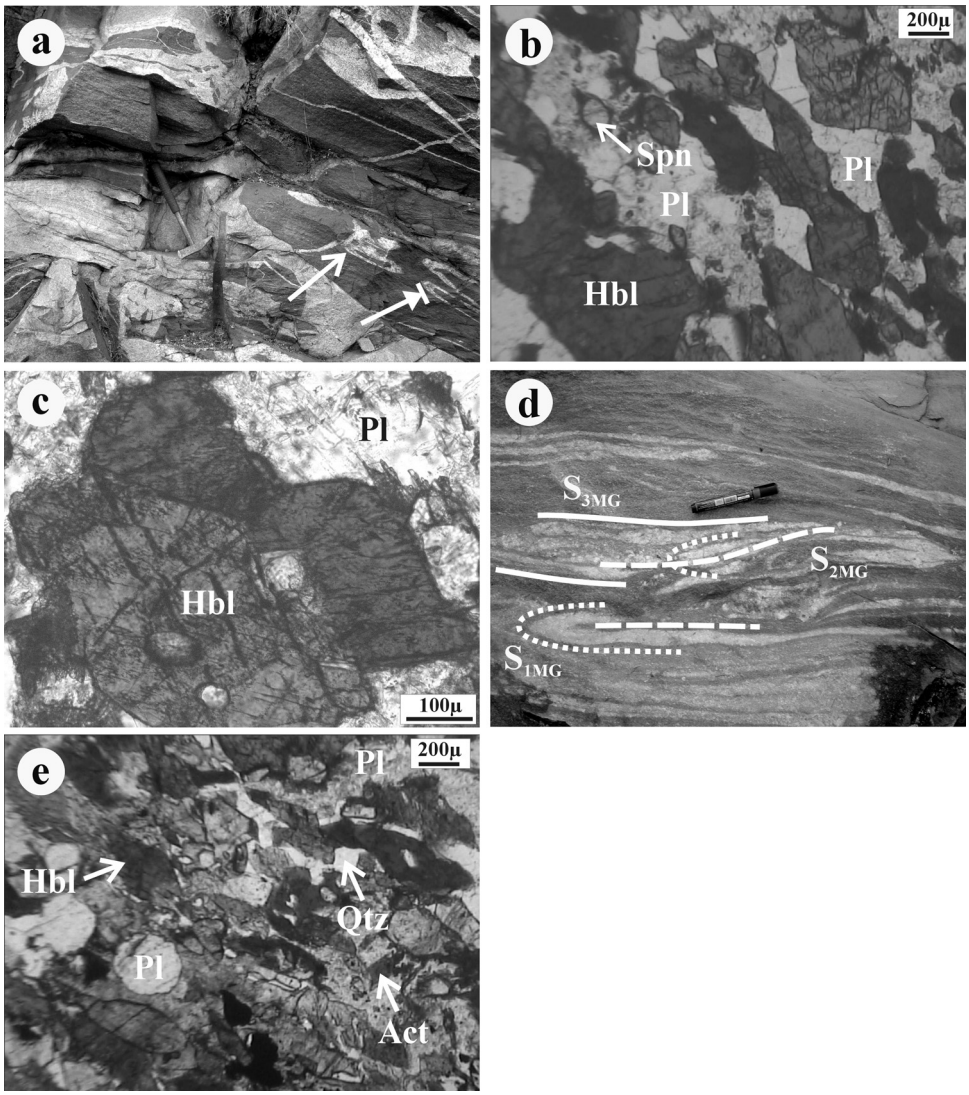

Fig. 6. Field photographs (a, d) and plane polarized microphotographs of textural relations (b, c and e) in Peninsular gneisses. (a) Section view showing gneissic layering (S_{3MG}) in migmatitic gneiss (Peninsular gneiss). The inter-layer penetrative foliation in gneiss (S_{2MG}) is axial planar to isoclinal folds (arrow with bar) and parallel to long axes of eye shaped (arrow) folds on leucocratic segregations (S_{1MG}). (b) Platy granoblastic texture defined by polygonized aggregates of hornblende (darker shade) anchored to annealed plagioclase (lighter shade) in melanocratic layer in Peninsular gneiss (sphene indicated by arrow). (c) Close up view of melanocratic layer showing triple junction among hornblende anchored to recrystallized plagioclase. (d) Plan view of the Peninsular gneiss (pen: 15 cm long; pen-head points north) showing both isoclinal folds on S_{1MG} leucosome layers (dotted line) and axial planar S_{2MG} fabric (broken line) drawn into parallelism with S_{3MG} fabric (continuous line). (e) Fine-grained intergrowths of actinolite-chlorite-epidote replacing aggregates of coarser-grained hornblende and plagioclase defining S_{2MG} in melanocratic layer in Peninsular gneiss. Note polygonized plagioclase grains are rounded by the replacement reactions. Calcite is often an accessory phase. Mineral abbreviations are from Kretz (1983), unless otherwise specified.

chlorite-muscovite schist, and amphibolite (Fig. 9b); granitoids and gneisses constitute more rounded/elliptical clasts (Fig. 9a).

The penetrative fabric in the para-schists/phyllites is defined by fine-grained chlorite-biotite aggregates (Fig. 9c); the fabric in deformed conglomerates is sub-greenschist facies and stylolitic, with prominent quartz, calcite beards in strain shadow zones of clasts (Fig. 9d). In the absence of preceding tectonic fabric barring local crenulations in strain shadow zones of clasts in conglomerates, the penetrative tectonic fabric in GSB designated S_{1GO} ('GO' for Goa schist belt) is inferred to be the earliest fabric. S_{1GO} is frequently crenulated, but the corresponding axial planar fabric (S_{2GO}) defined by neo-crystallized muscovite-chlorite aggregates is weakly developed through out the Goa schist belt (Fig. 9c and d). In regional scale, poles to S_{1GO} describe a well-defined girdle (Fig. 8). The β-axis of the girdle plunging at low angle toward SE/SSE and N/NNW broadly corresponds with the measured plunges of asymmetric upright F_{2GO} folds (Fig. 8). E-trending F_{3GO} crenulations on S_{1GO} mark the last deformation event in the GSB (Fig. 9a).

3.4. Granitoids

Granitoids occur as (i) medium-grained, equigranular and mesocratic tonalite-granodiorite dykes (Fig. 10a and b) in Peninsular gneiss, and (ii) coarse-grained, leucocratic blastoporphyritic granodiorite (Fig. 10c) occurring as apophyses and plutons that intrude Peninsular gneisses, tonalite granitoids (Fig. 10a) and supracrustals. The granitoid dykes contain angular rafts of Peninsular gneisses (Fig. 10a) and truncate the S_{3MG} fabric in these gneisses (Fig. 10b). In the mesocratic dykes, the internally strained plagioclase and K-feldspar grains (deformation bands, undulatory extinction, and sub-grains) that comprise the equigranular mosaic share high energy (serrated to plumose) grain/phase boundaries. By contrast, plagioclase in blastoporphyritic granitoids is weakly deformed and largely preserves euhedral/subhedral magmatic shape (Fig. 10d). Magmatic plagioclase crystals locally aligned in the polygonized matrix of K-feldspar and quartz (Fig. 10d) are reminiscent of magmatic flow textures. Evidence of internal plastic strain in feldspars is

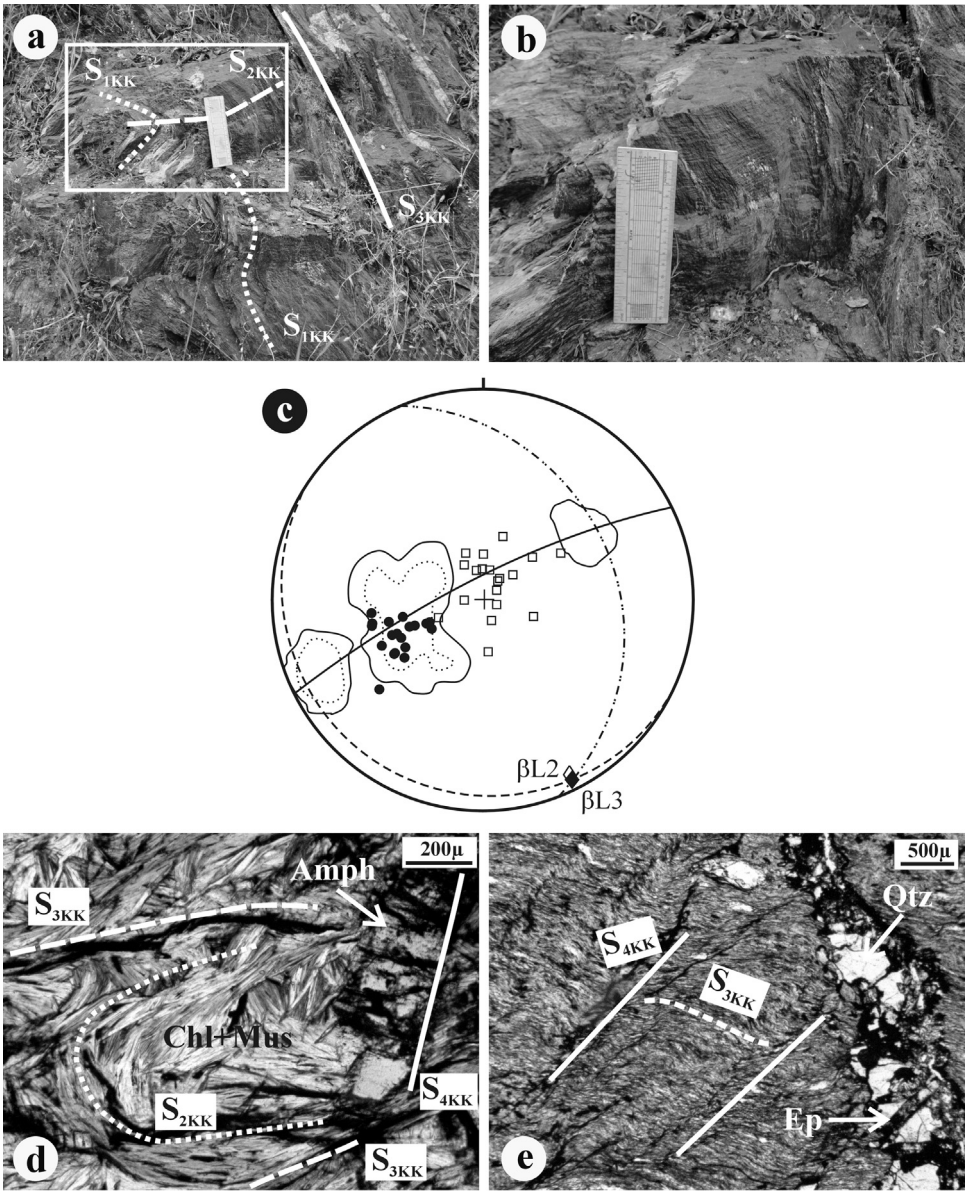

Fig. 7. Fabric relations in the Karwar-Kumta schists: (a, b) field photos, (c) stereographic plot, and (d, e) optical images. (a) Perspective view (looking NW) of a ~1 m wide "microlithon" in quartz-mica schist from the Kudremukh National Park (exact location in text). The warping foliation to the "microlithon" is the penetrative S_{3KK} foliation (continuous line). In the S_{3KK} interfolial domain, early foliation S_{1KK} (dotted line) is crenulated and the sub-horizontal crenulation cleavage (S_{2KK}; broken line) is truncated by the S_{3KK} fabric. (b) Close up view of the "microlithon" shown with white box in (a), but lines are avoided to preserve clarity. (c) Stereographic projection of foliation data measured in the outcrop (a, b). Poles to S_{1KK} ($n = 24$) contoured at intervals of 5% (continuous line) and 10% (dotted line) (Max ~ 21%) describe ENE-WSW pole girdle; the axis corresponding to the girdle (βL2; open diamond) indicated. Poles to S_{2KK} (open squares; $n = 18$) and the corresponding mean girdle of gentle SW-dipping S_{2KK} (broken line) are shown. Poles to the warping S_{3KK} foliation (filled circles; $n = 17$) and the mean girdle of NNW-trending ESE-dipping S_{3KK} foliation (dash-dot line) are shown. F_{3KK} fold axis is designated βL3 (filled diamond). (d) Chlorite-actinolite schist showing folded interfolial chlorite-defined S_{2KK} fabric, warping crenulation cleavage S_{3KK}, and weakly developed S_{4KK} cleavage defined by prismatic actinolite (Amph). (e) Weak crenulations on S_{3KK} fabric in Bt-Mus schist and development of associated S_{4KK} disjunctive shears axial planar to the crenulations. Epidote crystals in quartz veins growing inward from the vein wall grew by dissolution-precipitation in fractures oriented parallel to the instantaneous stretching axes of the en echelon shears.

manifested by sub-grain rotation recrystallization along margins of magmatic plagioclase crystals, and weak undulatory extinction in the core (Fig. 10d). By contrast, strain wavy extinction, deformation bands, and high-energy grain boundaries characterize polygonized quartz lentils defining the foliation (Fig. 10d).

3.5. Synthesis of structural relations

The non-planar and non-cylindrical set of open to close, N/NNW-trending, upright and sub-horizontal to gently plunging asymmetric folds ($F_{2GO} \approx F_{4MG} \approx F_{4KK}$) affecting the gneisses, both supracrustal belts, and presumably the deformed Karwar-Chauri and Londa blastoporphyritic granitoid plutons, provides a convenient starting point for structural correlation among the different lithodemic units. The mineralogy of chlorite-mica and chlorite-actinolite aggregates defining the axial planar fabric associated with this folding event suggests the deformation occurred at greenschist facies conditions. The low-T of deformation is corroborated by microstructures in the blastoporphyritic granitoids, e.g. intense dynamic recrystallization in K-feldspar, but plagioclase porphyries largely preserve their magmatic shapes, and are at best, weakly strained (Fig. 10d). Plastic deformation in K-feldspar is initiated at 400–450 °C for a wide range of fluid pressure and strain rate (Simpson, 1985), and brittle-ductile transition in plagioclase occurs

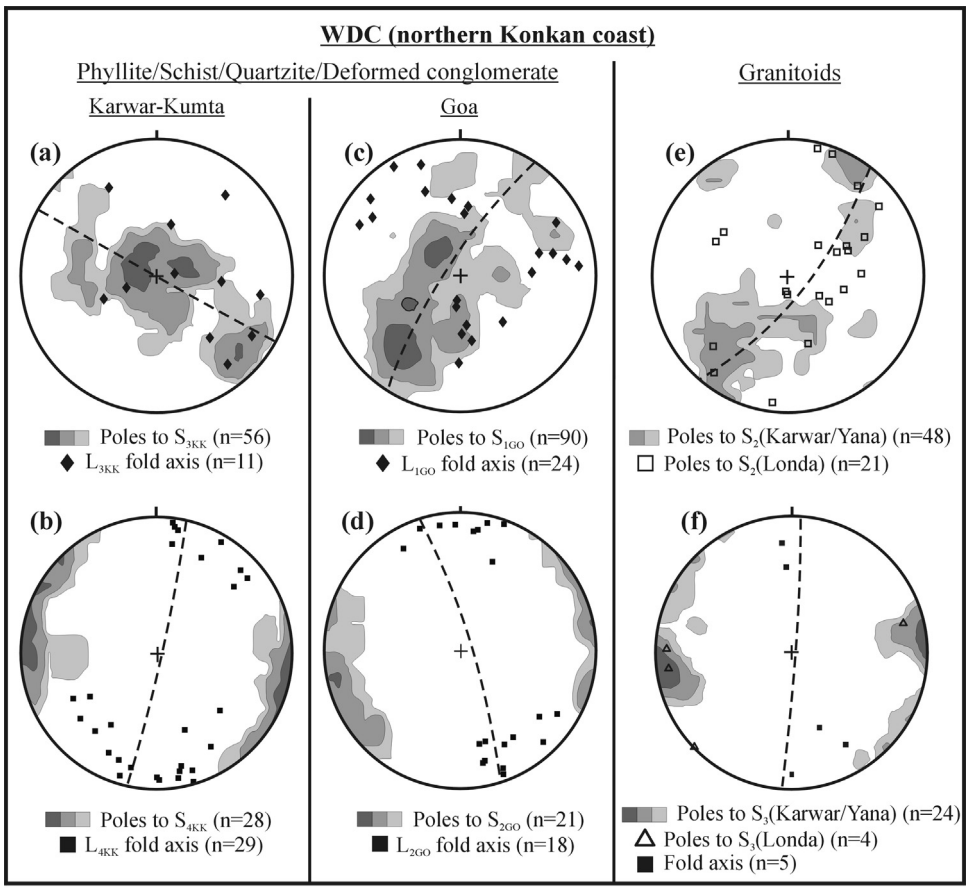

Fig. 8. Stereographic plot of structural elements in (a, b) the Karwar-Kumta schist belt, (c, d) the Goa schist belt, and (e, f) Karwar, Yana and Londa blastoporphyritic granitoids. (a) Pole girdle of S_{3KK} ($n = 56$) contoured at intervals of 2%, 4% and 8% (in increasing shades of gray; Max = 11.86%) and the filled diamonds are L_{3KK} fold axis ($n = 11$). (b) Poles to S_{4KK} ($n = 28$) contoured at intervals of 4%, 8% and 16% (in increasing shades of gray; Max ~ 32%) and the filled rectangles are L_{4KK} fold axis ($n = 29$). (c) Poles to S_{1GO} ($n = 90$) contoured at intervals of 2%, 4% and 8% (in increasing shades of gray; Max = 13%) and the filled diamonds are undifferentiated L_{1GO} fold axis ($n = 24$). (d) Poles to S_{2GO} ($n = 21$) contoured at intervals of 5%, 10% and 20% (in increasing shades of gray; Max = 24%) and the filled rectangles are L_{2O} fold axis ($n = 18$). (e) Poles to S_2 (Karwar/Yana granitoids) ($n = 48$) contoured at intervals of 3% and 6% (in increasing shades of gray; Max ~ 10%) and poles to S_2 (Londa granitoid) ($n = 21$) has shown with open rectangles. (f) Pi poles of S_3 (Karwar/Yana granitoids) ($n = 24$) contoured at intervals of 5%, 10% and 20% (in increasing shades of gray; Max = 33%) and the poles to S_3 (Londa granitoid) ($n = 4$) shown by open triangles. The filled rectangles are fold axis ($n = 5$).

at somewhat higher temperature, e.g. >450–500 °C (Lafrance and Vernon, 1999). Clearly the lithodemic units were deformed at temperature 450–500 °C bracketed by the brittle-ductile transition temperatures of K-feldspar and plagioclase. However, the mesoscopic features in Fig. 10 suggest that the equigranular and mesocratic granitoids, occurring as dykes in Peninsular gneisses and deformed above the brittle-ductile transition temperature of plagioclase, were emplaced earlier than the blastoporphyritic granitoids.

The fewer tectonic fabrics in the GSB para-schists relative to the Karwar-Kumta schists suggests that the Goa schist belt was either tectonically accreted to the migmatitic basement gneisses post-dating the tectonic accretion of Karwar-Kumta schist belt or unconformably overlies the basement gneisses and the Karwar-Kumta schist belt composite. Although the fold geometry in the two schist belts appears similar in regional scale, the orientations of axial planes and axes of the asymmetric folds in the two schist belts are different (Fig. 8). The obliquities arise due to the curvilinear nature of the axial plane of the folds, e.g. the axial planes of the asymmetric folds trending NNE in the southern part in the area curve to a more westerly orientation (NNW-trending) northwards in the region around Goa (Fig. 5) due to superposition of younger deformation events ($F_{3GO} \approx F_{5KK} \approx F_{5MG}$). If the axial planes of the asymmetric folds are restored to similar orientation, the pole girdles corresponding to S_{1GO} and S_{3KK} (Fig. 8) are not co-planar, i.e. the orientations of S_{1GO} in the Goa schist belt and the S_{3KK} Karwar-Kumta schist belts were different prior to E-W shortening that gave rise to asymmetric N-trending folds. The obliquity of pole girdles and the fewer tectonic fabrics in the Goa schist belt suggests the two supracrustal belts did not share a coherent crustal evolutionary history prior to the E-W crustal shortening event.

Several lines of evidence suggest the S_{1MG} and S_{2MG} fabrics in Peninsular gneisses formed at high-T anatectic conditions, e.g. the occurrence of biotite rimming leucosome layers (Fig. 6a), the assemblage of polygonized hornblende and plagioclase in the melanocratic S_{2MG} layers (Fig. 6b), and annealing recrystallization in hornblende forming triple junctions ($T > 650$ °C; Berger and Stünitz, 1996; Hacker and Christie, 1991) anchored to polygonized plagioclase grains (Fig. 6c). By contrast, chlorite-biotite-muscovite aggregates defining successive tectonic fabrics in the Karwar-Kumta schist belt imply the rocks were perpetually deformed at greenschist facies condition. We infer therefore that the Karwar-Kumta schists were tectonically accreted to the Peninsular gneisses post-dating the high-T fabric-forming deformation events in the gneisses.

4. Electron micro-probe (EMP) age determinations in monazite

All analyses were carried out with a CAMECA SX-100 electron probe microanalyzer equipped with 4 wavelength dispersive spectrometers in the Department of Geology and Geophysics, IIT

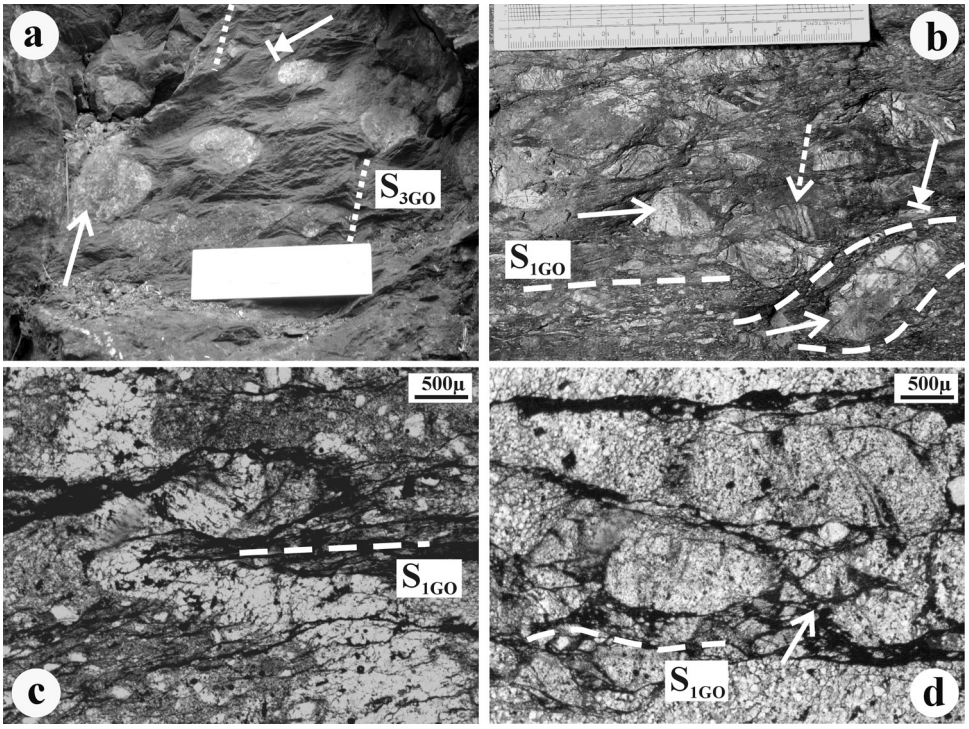

Fig. 9. (a, b) Poorly-sorted angular to sub-rounded clasts of Banded Iron Formations (broken arrow), amphibolites (arrow with bar), phyllite, gneiss, foliated granitoid (arrow) in deformed polymict para-conglomerates close to the margin of the Goa schist belt (Fig. 4). The penetrative foliation (from left to right) is S_{1GO} (see text for explanation). Ruler in (a) and (b) is ~15 cm long. In (a), trace of axial plane of weakly developed F_{3GO} crenulations is shown by broken line. In (b), the broken line shows S_{1GO} warping around a clast. (c) Wispy aggregates (S_{1GO}) of Chl and Mus axial planar to a folded quartz vein in phyllites. Note the absence of a preceding cleavage in the interfolial domain of S_{1GO}. The ellipsoidal light colored objects in the matrix are monomineralic quartz grains. (d) Stylolitic cleavage and "beard structure" (arrow) in deformed quartz conglomerate. The quartz clasts replaced by equant polygonized grains are sugary in appearance.

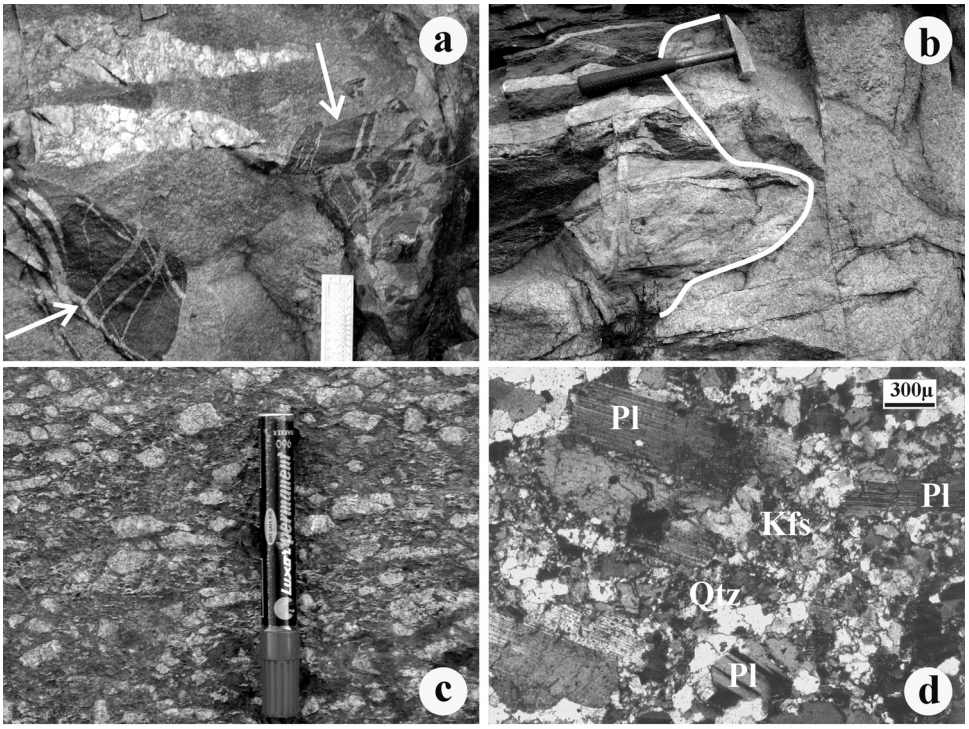

Fig. 10. Field appearances (a–c) and textural relation (d) in granitoids. (a) Rafts of Peninsular gneiss (arrows) in equigranular, mesocratic tonalite dyke. Note blastoporphyritic granitoid is intrusive into the tonalite dyke. Ruler is 15 cm long. (b) Peninsular gneiss intruded by equigranular, mesocratic tonalite dyke (contact between these two lithounits is shown with continuous line). Note the S_{3MG} gneiss layer in Peninsular gneiss is truncated by the intrusive tonalite dyke. (c) Appearance of foliated blastoporphyritic granitoid. Aggregates of polygonized K-feldspar grains and quartz lenticels warping around plagioclase porphyry define the tectonic fabric in blastoporphyritic granitoid. Note pressure shadow zones around porphyries. Pen: 15 cm long; pen-head points north. (d) Locally aligned laths of euhedral plagioclase (polysynthetic twins parallel to grain elongation) in a finer-grained mosaic of recrystallized quartz and K-feldspar in blastoporphyritic granitoid. Note (i) the lack of internal strain in plagioclase laths, and (ii) sub-grain along plagioclase margin.

Table 1
ThO_2, UO_2 and PbO concentrations, chemical spot ages, and 2σ error of spot ages in monazites (locations of monazite-dated samples in Figs. 2 and 4) obtained in this study. Electron probe microanalysis data on monazites are provided in Data Repository[1].

Spot age Ref. No:	ThO_2 (wt%)	UO_2 (wt%)	PbO (wt%)	Age (Ma)	Age err (±2σ)	Spot age Ref. No:	ThO_2 (wt%)	UO_2 (wt%)	PbO (wt%)	Age (Ma)	Age err (±2σ)
Blastoporphyritic granitoid (Karwar and Chauri)											
CAN-10 (Lat: 15° 00.920′ N Long: 74° 01.071′ E)											
$C_{1/1}$	3.50	0.24	0.62	2998	94	$C_{1/13}$	5.07	0.28	0.85	2994	73
$C_{1/2}$	3.65	0.22	0.62	2982	94	$C_{1/14}$	5.20	0.30	0.87	2961	71
$C_{1/3}$	3.67	0.25	0.64	2998	91	$C_{1/15}$	3.41	0.20	0.58	2983	99
$C_{1/4}$	9.84	0.33	1.48	2903	49	$C_{1/16}$	4.03	0.25	0.68	2933	84
$C_{1/5}$	13.96	0.45	2.08	2904	39	$C_{1/17}$	4.19	0.24	0.71	2989	85
$C_{1/6}$	12.19	0.35	1.80	2910	43	$C_{1/18}$	3.86	0.21	0.65	3030	92
$C_{1/7}$	8.25	0.30	1.27	2943	55	$C_{1/19}$	4.24	0.20	0.69	2971	86
$C_{1/8}$	6.20	0.19	0.90	2862	68	$C_{1/20}$	3.64	0.18	0.60	3002	97
$C_{1/9}$	6.41	0.23	0.99	2954	66	$C_{1/21}$	3.92	0.18	0.62	2941	93
$C_{1/10}$	3.46	0.20	0.59	3023	99	$C_{1/22}$	5.32	0.26	0.86	2962	73
$C_{1/11}$	4.17	0.17	0.67	3023	90	$C_{1/23}$	3.70	0.20	0.62	2995	95
$C_{1/12}$	3.80	0.23	0.65	2996	90						
KK-49C (Lat: 14° 47.361′ N Long: 74° 07.021′ E)											
$K_{1/1}$	9.18	0.38	1.41	2889	49	$K_{1/15}$	6.37	0.22	0.96	2916	66
$K_{1/2}$	6.86	0.36	1.13	2959	59	$K_{1/16}$	7.47	0.24	1.11	2893	59
$K_{1/3}$	7.95	0.34	1.25	2928	55	$K_{1/17}$	6.11	0.19	0.93	2961	70
$K_{1/4}$	7.89	0.31	1.22	2937	56	$K_{1/18}$	3.37	0.28	0.61	2952	91
$K_{1/5}$	9.82	0.30	1.46	2909	49	$K_{1/19}$	3.95	0.26	0.70	3036	87
$K_{1/6}$	7.25	0.25	1.10	2912	60	$K_{1/20}$	8.84	0.27	1.32	2920	53
$K_{1/7}$	6.40	0.20	0.97	2948	67	$K_{1/21}$	8.23	0.27	1.25	2941	55
$K_{1/8}$	6.05	0.19	0.91	2924	70	$K_{1/22}$	7.44	0.22	1.11	2919	60
$K_{1/9}$	10.31	0.36	1.57	2931	47	$K_{1/23}$	5.86	0.18	0.88	2936	71
$K_{1/10}$	8.42	0.31	1.29	2929	54	$K_{1/24}$	8.05	0.27	1.18	2839	55
$K_{1/11}$	8.64	0.26	1.29	2918	54	$K_{1/25}$	4.85	0.16	0.74	2974	83
$K_{1/12}$	10.88	0.33	1.60	2890	46	$K_{1/26}$	4.43	0.18	0.69	2941	86
$K_{1/13}$	14.73	0.43	2.18	2908	38	$K_{1/27}$	5.75	0.20	0.87	2928	72
$K_{1/14}$	7.48	0.24	1.13	2939	59	$K_{1/28}$	3.78	0.14	0.59	2952	99
KK-47 (Lat: 14° 48.190′ N Long: 74° 07.494′ E)											
$K_{2/1}$	4.70	0.20	0.76	3005	82	$K_{2/8}$	4.44	0.08	0.64	2970	94
$K_{2/2}$	6.46	0.31	1.05	2964	63	$K_{2/9}$	4.72	0.09	0.69	2983	89
$K_{2/3}$	6.02	0.31	0.99	2976	66	$K_{2/10}$	4.49	0.18	0.70	2947	84
$K_{2/4}$	5.29	0.34	0.89	2902	68	$K_{2/11}$	6.45	0.33	1.04	2930	62
$K_{2/5}$	4.51	0.24	0.77	3044	82	$K_{2/12}$	5.20	0.34	0.88	2917	69
$K_{2/6}$	4.69	0.22	0.78	3026	81	$K_{2/13}$	6.43	0.31	1.04	2943	62
$K_{2/7}$	5.75	0.17	0.85	2915	73	$K_{2/14}$	5.44	0.15	0.82	2968	77
KK-50 (Lat: 14° 46.924′ N Long: 74° 08.443′ E)											
$K_{3/1}$	10.86	0.32	1.60	2889	46	$K_{3/6}$	11.82	0.34	1.73	2886	43
$K_{3/2}$	11.17	0.30	1.59	2839	45	$K_{3/7}$	11.93	0.32	1.74	2901	44
$K_{3/3}$	10.39	0.26	1.51	2897	48	$K_{3/8}$	11.50	0.32	1.74	2979	45
$K_{3/4}$	12.04	0.32	1.83	3015	44	$K_{3/9}$	11.37	0.34	1.65	2850	44
$K_{3/5}$	16.97	0.32	2.32	2809	35	$K_{3/10}$	15.01	0.25	2.12	2911	39
Blastoporphyritic granitoid (Quepem)											
CHA-4 (Lat: 15° 11.954′ N Long: 74° 02.143′ E)											
$C_{2/1}$	13.70	0.76	1.96	2594	35	$C_{2/10}$	11.75	0.67	1.68	2586	38
$C_{2/2}$	20.77	0.99	2.83	2553	28	$C_{2/11}$	12.39	0.69	1.79	2619	37
$C_{2/3}$	12.34	0.69	1.75	2581	37	$C_{2/12}$	12.78	0.52	1.66	2500	37
$C_{2/4}$	11.77	0.66	1.64	2540	38	$C_{2/13}$	12.51	0.37	1.60	2549	39
$C_{2/5}$	20.43	0.76	2.72	2579	29	$C_{2/14}$	20.09	0.77	2.70	2588	29
$C_{2/6}$	12.18	0.68	1.73	2582	37	$C_{2/15}$	13.26	0.35	1.64	2506	38
$C_{2/7}$	13.51	0.22	1.69	2614	39	$C_{2/16}$	11.40	0.33	1.45	2537	42
$C_{2/8}$	17.07	0.68	2.24	2526	31	$C_{2/17}$	11.74	0.31	1.50	2581	42
$C_{2/9}$	12.63	0.70	1.78	2570	36						

Phyllite/schist (Goa schist belt)

ZEN-44C (Lat: 15° 31.981′ N Long: 74° 05.709′ E)

$Z_{1/1}$	3.89	0.05	0.45	2450	95	$Z_{1/11}$	4.61	0.02	0.50	2398	102
$Z_{1/2}$	4.03	0.06	0.48	2501	94	$Z_{1/12}$	4.07	0.03	0.46	2457	113
$Z_{1/3}$	2.58	0.06	0.32	2512	132	$Z_{1/13}$	3.29	0.01	0.35	2334	122
$Z_{1/4}$	4.52	0.06	0.53	2493	84	$Z_{1/14}$	4.42	0.03	0.50	2443	108
$Z_{1/5}$	3.38	0.05	0.38	2383	107	$Z_{1/15}$	3.03	0.04	0.34	2416	142
$Z_{1/6}$	2.83	0.05	0.32	2375	123	$Z_{1/16}$	4.39	0.01	0.48	2414	101
$Z_{1/7}$	3.89	0.11	0.47	2406	92	$Z_{1/17}$	4.98	0.02	0.53	2363	98
$Z_{1/8}$	4.11	0.11	0.49	2408	88	$Z_{1/18}$	2.70	0.02	0.31	2526	150
$Z_{1/9}$	3.49	0.00	0.37	2384	108	$Z_{1/19}$	3.80	0.02	0.42	2406	113
$Z_{1/10}$	4.52	0.01	0.49	2425	98						

ZEN-45C (Lat: 15° 31.613′ N Long: 74° 06.115′ E)

$Z_{2/1}$	2.76	0.04	0.35	2639	132	$Z_{2/20}$	4.90	0.06	0.58	2533	80
$Z_{2/2}$	3.56	0.05	0.44	2588	108	$Z_{2/21}$	3.69	0.07	0.43	2425	98
$Z_{2/3}$	3.87	0.05	0.47	2580	99	$Z_{2/22}$	3.24	0.02	0.36	2415	139
$Z_{2/4}$	2.40	0.04	0.30	2631	151	$Z_{2/23}$	4.98	0.02	0.56	2476	111
$Z_{2/5}$	4.78	0.07	0.58	2547	83	$Z_{2/24}$	3.74	0.03	0.42	2414	130
$Z_{2/6}$	3.81	0.11	0.48	2530	96	$Z_{2/25}$	4.83	0.02	0.53	2429	110
$Z_{2/7}$	3.22	0.05	0.40	2633	118	$Z_{2/26}$	5.19	0.03	0.59	2491	112
$Z_{2/8}$	2.51	0.04	0.32	2648	144	$Z_{2/27}$	5.02	0.03	0.60	2602	116
$Z_{2/9}$	3.75	0.06	0.46	2546	101	$Z_{2/28}$	3.88	0.03	0.46	2548	131
$Z_{2/10}$	3.93	0.08	0.48	2506	96	$Z_{2/29}$	4.53	0.02	0.51	2456	115
$Z_{2/11}$	3.31	0.11	0.41	2454	105	$Z_{2/30}$	3.19	0.01	0.39	2662	141
$Z_{2/12}$	2.58	0.06	0.34	2675	138	$Z_{2/31}$	4.60	0.00	0.54	2630	104
$Z_{2/13}$	4.71	0.07	0.59	2621	86	$Z_{2/32}$	4.00	0.00	0.48	2678	117
$Z_{2/14}$	2.56	0.05	0.30	2430	137	$Z_{2/33}$	3.14	0.01	0.36	2547	140
$Z_{2/15}$	3.66	0.05	0.47	2680	106	$Z_{2/34}$	3.60	0.00	0.43	2649	114
$Z_{2/16}$	3.73	0.05	0.47	2648	103	$Z_{2/35}$	3.19	0.01	0.37	2574	136
$Z_{2/17}$	2.49	0.04	0.32	2681	139	$Z_{2/36}$	3.40	0.01	0.40	2568	136
$Z_{2/18}$	3.29	0.05	0.42	2672	116	$Z_{2/37}$	2.25	0.00	0.26	2566	139
$Z_{2/19}$	5.00	0.06	0.60	2567	80						

ZEN-39A & B (Lat: 15° 02.757′ N Long: 74° 01.618′ E)

$Z_{3/1}$	4.68	0.22	0.68	2683	108	$Z_{3/4}$	3.38	0.12	0.44	2546	132
$Z_{3/2}$	4.31	0.09	0.56	2694	119	$Z_{3/5}$	3.41	0.09	0.44	2588	135
$Z_{3/3}$	3.62	0.17	0.48	2505	122	$Z_{3/6}$	3.68	0.08	0.47	2598	130

Phyllite/schist (Karwar-Kumta schist belt)

KK-79A (Lat: 14° 17.546′ N Long: 74° 30.264′ E)

$K_{4/1}$	11.88	0.33	1.85	3064	45	$K_{4/4}$	11.24	0.24	1.73	3095	70
$K_{4/2}$	11.80	0.32	1.84	3075	45	$K_{4/5}$	4.69	0.04	0.65	2962	117
$K_{4/3}$	10.81	0.24	1.69	3122	73	$K_{4/6}$	4.85	0.04	0.68	2988	114

KK-115 (Lat: 14° 44.362′ N Long: 74° 40.306′ E)

$K_{5/1}$	1.94	0.09	0.33	3097	161	$K_{5/5}$	6.10	0.22	0.93	2930	144
$K_{5/2}$	4.26	0.11	0.69	3191	98	$K_{5/6}$	5.56	0.07	0.86	3205	165
$K_{5/3}$	3.57	0.11	0.55	2992	108	$K_{5/7}$	5.60	0.07	0.85	3165	163
$K_{5/4}$	7.87	0.61	1.49	3105	122						

Clasts in deformed polymict conglomerate (Goa schist belt)

ZEN-31Cx & Cy (Lat: 15° 15.115′ N Long: 74° 01.181′ E)

$Z_{4/1}$	5.19	0.30	0.94	3167	73	$Z_{4/14}$	9.27	0.27	1.48	3109	53
$Z_{4/2}$	5.70	0.25	0.97	3124	71	$Z_{4/15}$	8.20	0.34	1.37	3093	55
$Z_{4/3}$	7.65	0.55	1.45	3157	53	$Z_{4/16}$	8.42	0.25	1.35	3117	57

Table 1 (*Continued*)

Spot age Ref. No:	ThO_2 (wt%)	UO_2 (wt%)	PbO (wt%)	Age (Ma)	Age err (±2σ)	Spot age Ref. No:	ThO_2 (wt%)	UO_2 (wt%)	PbO (wt%)	Age (Ma)	Age err (±2σ)
$Z_{4/4}$	5.89	0.32	1.06	3187	67	$Z_{4/17}$	10.46	0.70	1.93	3122	42
$Z_{4/5}$	5.58	0.25	0.94	3116	73	$Z_{4/18}$	7.00	0.23	1.10	3026	63
$Z_{4/6}$	4.60	0.14	0.75	3175	89	$Z_{4/19}$	4.15	0.16	0.71	3196	94
$Z_{4/7}$	4.47	0.13	0.75	3238	92	$Z_{4/20}$	9.31	0.28	1.44	3012	52
$Z_{4/8}$	5.90	0.32	1.06	3167	67	$Z_{4/21}$	8.67	0.16	1.32	3102	93
$Z_{4/9}$	6.90	0.12	1.02	3032	67	$Z_{4/22}$	8.64	0.17	1.32	3098	93
$Z_{4/10}$	7.70	0.19	1.22	3136	62	$Z_{4/23}$	7.00	0.04	1.02	3132	99
$Z_{4/11}$	5.63	0.28	1.02	3232	71	$Z_{4/24}$	3.83	0.26	0.71	3143	89
$Z_{4/12}$	5.37	0.18	0.89	3155	78	$Z_{4/25}$	3.59	0.26	0.71	3251	92
$Z_{4/13}$	6.32	0.23	1.07	3188	69						
Peninsular gneiss											
JD-2 (Lat: 15° 10.001′ N Long: 74° 29.700′ E)											
$J_{1/1}$	4.63	0.06	0.71	3198	95	$J_{1/7}$	5.09	0.06	0.78	3215	89
$J_{1/2}$	4.73	0.05	0.70	3120	93	$J_{1/8}$	5.04	0.06	0.76	3123	88
$J_{1/3}$	4.36	0.05	0.65	3107	99	$J_{1/9}$	5.43	0.07	0.83	3181	84
$J_{1/4}$	5.28	0.07	0.80	3127	85	$J_{1/10}$	4.62	0.04	0.67	3058	94
$J_{1/5}$	5.52	0.07	0.84	3187	83	$J_{1/11}$	5.39	0.07	0.83	3193	85
$J_{1/6}$	5.54	0.08	0.85	3146	82	$J_{1/12}$	5.29	0.07	0.81	3168	85
ZEN-8 (Lat: 12° 56.185′ N Long: 74° 51.646′ E)											
$Z_{5/1}$	4.48	0.04	0.68	3177	97	$Z_{5/10}$	8.23	0.09	1.22	3111	61
$Z_{5/2}$	4.73	0.04	0.71	3178	94	$Z_{5/11}$	8.26	0.10	1.22	3094	60
$Z_{5/3}$	4.93	0.06	0.74	3135	90	$Z_{5/12}$	7.17	0.08	1.07	3125	67
$Z_{5/4}$	5.06	0.07	0.77	3148	87	$Z_{5/13}$	6.47	0.08	0.96	3109	72
$Z_{5/5}$	9.25	0.12	1.39	3133	56	$Z_{5/14}$	8.64	0.09	1.28	3120	59
$Z_{5/6}$	5.30	0.07	0.82	3183	86	$Z_{5/15}$	5.98	0.08	0.90	3129	77
$Z_{5/7}$	5.20	0.07	0.79	3161	86	$Z_{5/16}$	4.55	0.05	0.69	3183	96
$Z_{5/8}$	5.97	0.08	0.89	3117	77	$Z_{5/17}$	4.67	0.07	0.71	3140	93
$Z_{5/9}$	8.76	0.10	1.30	3115	58						
Matrix in deformed polymict conglomerate (Goa schist belt)											
ZEN-36B (Lat: 15° 03.761′ N Long: 74° 03.244′ E)											
$Z_{6/1}$	3.70	0.07	0.46	2588	101	$Z_{6/5}$	2.52	0.06	0.30	2396	132
$Z_{6/2}$	6.30	0.08	0.74	2487	67	$Z_{6/6}$	2.84	0.00	0.31	2414	113
$Z_{6/3}$	6.31	0.08	0.73	2451	66	$Z_{6/7}$	3.21	0.04	0.37	2471	132
$Z_{6/4}$	6.23	0.07	0.71	2434	66						
ZEN-36D (Lat: 15° 03.761′ N Long: 74° 03.244′ E)											
$Z_{7/1}$	2.55	0.04	0.31	2539	138	$Z_{7/7}$	4.42	0.04	0.53	2586	113
$Z_{7/2}$	3.57	0.08	0.44	2512	116	$Z_{7/8}$	4.27	0.04	0.48	2407	112
$Z_{7/3}$	4.55	0.07	0.56	2575	87	$Z_{7/9}$	3.47	0.04	0.42	2608	135
$Z_{7/4}$	3.97	0.05	0.47	2511	95	$Z_{7/10}$	3.49	0.03	0.39	2426	126
$Z_{7/5}$	3.05	0.08	0.39	2595	128	$Z_{7/11}$	3.61	0.01	0.42	2577	116
$Z_{7/6}$	2.77	0.05	0.32	2439	124						

Kharagpur, India. Monazites were analyzed using 20 kV acceleration voltage and 200 nA beam current, but calibration was performed with acceleration voltage 20 kV and 20 nA beam current. SiK_α, AlK_α, FeK_α, PK_α and CaK_α were calibrated using natural mineral standards. REEs (LaL_α, CeL_α, PrL_β, NdL_β, SmL_α, GdL_β, DyL_α, HoL_β) were calibrated using synthetic silica-aluminum glass, and yttrium-aluminum garnet (YAG) was used for yttrium (YL_α). Synthetic standards were used for ThM_α, UM_β and PbM_α. ThO_2 and UO_2 were used for Th and U respectively. Vanadinite [$(Pb_5(VO_4)_3Cl$] is selected as the standard for Pb instead of galena to avoid interferences of Pb and S (Scherrer et al., 2000). Integral mode in pulse-height analyzers was adopted for all elements, and matrix effects were corrected for by using X-PHI method (Merlet, 1992). The spectral interference of Y$L\gamma_2$, Y$L\gamma_3$ on PbM_α and Th$M\gamma$, ThM_3N_4 on UM_β was corrected during quantification. Pb was overestimated by ~35 ppm per wt% Y, and ThM2-O4, ThMζ1 and ThMζ2 together contribute 34 ppm Pb for 12 wt% Th (Jercinovic and Williams, 2005). In view of the fact that an overwhelming number of analyzed monazites contain ≪3 wt% Y_2O_3 and ≪12 wt% ThO_2 (Table 1), these corrections contribute marginally to total Pb estimation, and were ignored. The interference of LaL_α spectral line on PbM_α (Jercinovic and Williams, 2005) was not determined. Detection limits were calculated using the formulation developed by Ancey et al. (1978). The detection limits were 110, 330 and 170 ppm for Pb, Th and U respectively.

Pb, U and Th were simultaneously analyzed with LPET and PET crystals to enhance the number of counts. In this approach the counting times on LPET, PET crystals were respectively, 300 s, 180 s for PbM_α, 200 s and 120 s individually for ThM_α and UM_β, with half of the peak time assigned for background measurement. Exponential background fit for PbM_α was adopted for achieving better fit to the curvature of background values measured far away from peak position below the Pb peak (Jercinovic and Williams, 2005; Spear et al., 2009; Williams et al., 2006, 2007). The following overlaps, e.g. SiK_α on UM$_\beta$, GdL_α on UM_β, ThM_α, PbM_α and PrL_β on UM_β, ThM_α, PbM_α were examined and neglected due to ineffectiveness. Pb, Th and U were analyzed using the 'sub-counting' method to minimize sample surface damage (details of method in Spear et al., 2009); for the method, background and peak measurement were done in 10 cycles, and Chi^2 test was performed on the measurements to remove the inconsistent values, and final result was used for the age quantification (Spear et al., 2009). The new adjustments yielded the detection limits to be 90 ppm, 135 ppm and 115 ppm on Pb, Th and U respectively. The detection limits improved by 18% for Pb, 60% for Th and 32% for U over the corresponding values (quoted earlier) obtained without employing the above corrections.

The analytical protocol was tested and compared on two monazite standards (courtesy N. Chatterjee, Electron Microprobe Facility, Department of Earth, Atmospheric and Planetary Sciences, Massachusetts Institute of Technology). One of the standards is a pegmatite-hosted monazite (JCA-8 M09 and M10) from the Mount Narryer complex, Australia (TIMS age of 3132 ± 1 Ma; Chatterjee and Nicolaysen, 2012; Crowley et al., 2005). The other consists of three grains from the 'Moacyr' monazite (JCA-8) from Brazil. Thermal ionization mass spectrometry (TIMS) yielded $^{207}Pb/^{235}U$ = 483.1 ± 1.0 Ma and $^{206}Pb/^{238}U$ = 487.5 Ma ages for the sample (Crowley et al., 2005). Spear et al. (2009) obtained a TIMS age 509.3 ± 0.5 Ma for the Moacyr monazite. The age of the Mt. Narryer sample is close to the ages of rocks investigated in this study. For the Moacyr monazite, the estimated abundances of U and Th using the protocol agree with the TIMS values (Crowley et al., 2005) and EPM values (Spear et al., 2009), but Pb abundances obtained for the Moacyr monazite agree with those obtained by Spear et al. (2009). The cumulative probability plot with weighted-age of spot ages obtained using the formulation of Montel et al. (1996) yield 3118 ± 28 (n = 13) and 516 ± 12 Ma (n = 17) for the Mt. Narryer and the Moacyr monazite standards respectively ('n' is the number of spot ages). Details of analytical protocol and analytical results in the two standard samples are provided in Prabhakar (2013).

In this study, 240 monazite spot ages in 17 samples (locations in Fig. 4) are reported. The 2σ errors associated with the spot ages in the range between 2334 ± 122 Ma and 3196 ± 94 Ma (Table 1) are variable, e.g. 30–95 Ma (in granitoids), 60–97 Ma (in Peninsular gneisses), 42–100 Ma (in clasts in conglomerates). The 2σ errors in phyllites and schists are higher, e.g. 45–164 Ma (in the Karwar-Kumta schist belt) and 80–142 Ma (in the Goa schist belt). The % error [100 × (2σ error in Ma/absolute age in Ma)] in monazite spot ages (this study) increase with decreasing abundances of U, Th and Pb (Fig. 11). Vlach (2010) demonstrates that 2σ errors in spot ages are inversely correlated with the Th contents in monazite.

The % errors increase sharply at Th < 20,000 ppm, U < 1000 ppm and Pb < 2000 ppm The variations in the % error of spot ages with Th, U and Pb abundances (this study; Fig. 11d–f and Table 1) closely conform to the trends described by spot age data culled from the literature (Fig. 11a–c) in rocks older than 2000 Ma. The spot age errors (±2σ) reported by Mahan et al. (2006) are among the lowest known for Archean rocks (% error < 1.0%; not shown in Fig. 11). In the samples investigated by Mahan et al. (2006) for the age range 2462 ± 16 Ma–2593 ± 15 Ma, the abundances of Th, U and Pb are >27,000 ppm, >1700 ppm and >3800 ppm respectively. At these minimum values, the 2σ errors in the samples dated (this study) are higher relative to Mahan et al. (2006) by factors between 2.0 and 3.0; at higher Th, U and Pb abundances the 2σ errors are ~1.0 and 1.5 times the values quoted by Mahan et al. (2006). The % errors vary from 1% to 6% for the data sets of Cocherie and Albarede (2001), Duclaux et al. (2008), Goncalves et al. (2004), Loehn (2011) and Tickyj et al. (2004) (Fig. 11a–c). The % error in spot ages reported by Braun et al. (1998), Halpin et al. (2007) and Hokada et al. (2012; only 1σ error reported) are higher, e.g. ~7–16%, ~4–8% and ~2–37% respectively (Fig. 11a–c). Overall, the 2σ errors of our spot age data are better than, or comparable, with these estimates (Fig. 11).

In phyllites, schists and quartzites, the large errors associated with spot ages (Fig. 11d–f and Table 1) are problematic because (i) monazites with polygenetic history within the stated uncertainties cannot be resolved, and (ii) the mean age obtained from a population of monazites with un-resolved polygenetic history may not be significant. It is important therefore to identify if all analytical errors are adequately accounted. In this context, the age data in sample KK-79A from the Karwar-Kumta schist belt is instructive. In this sample, small (max. length: 10 μm) and chemically un-zoned monazite grains with high contents of ThO_2 (11.24–11.88 wt%), UO_2 (0.24–0.33 wt%) and PbO (1.73–1.85 wt%) yield three spot ages tightly constrained between 3064 and 3095 Ma, with 2σ errors between 45 and 73 Ma. In the same sample, two spot ages with larger errors, e.g. 2962 ± 117 Ma and 2988 ± 114 Ma are determined in two chemically homogenous low-Th monazite grains (ThO_2: 4.69–4.85 wt%). For the quoted errors, the two age populations are statistically indistinguishable (see below), and the larger age errors in low-Th monazites are due to the propagation of larger analytical errors at low abundances of Th, Pb and U (cf. Vlach, 2010). Apparently these larger analytical errors are induced by the attenuation in peak intensities at low concentrations of U, Pb and Th (Fig. 11) closer to the detection limits of the elements and/or errors in extrapolating peak/background ratios from high-Th, U and Pb standards (used in calibration) to samples (for age determination) having low abundances of these elements.

The probability density distribution of the spot ages computed using Isoplot/Ex (Ludwig, 2003) is presented for the individual samples (Fig. 12).

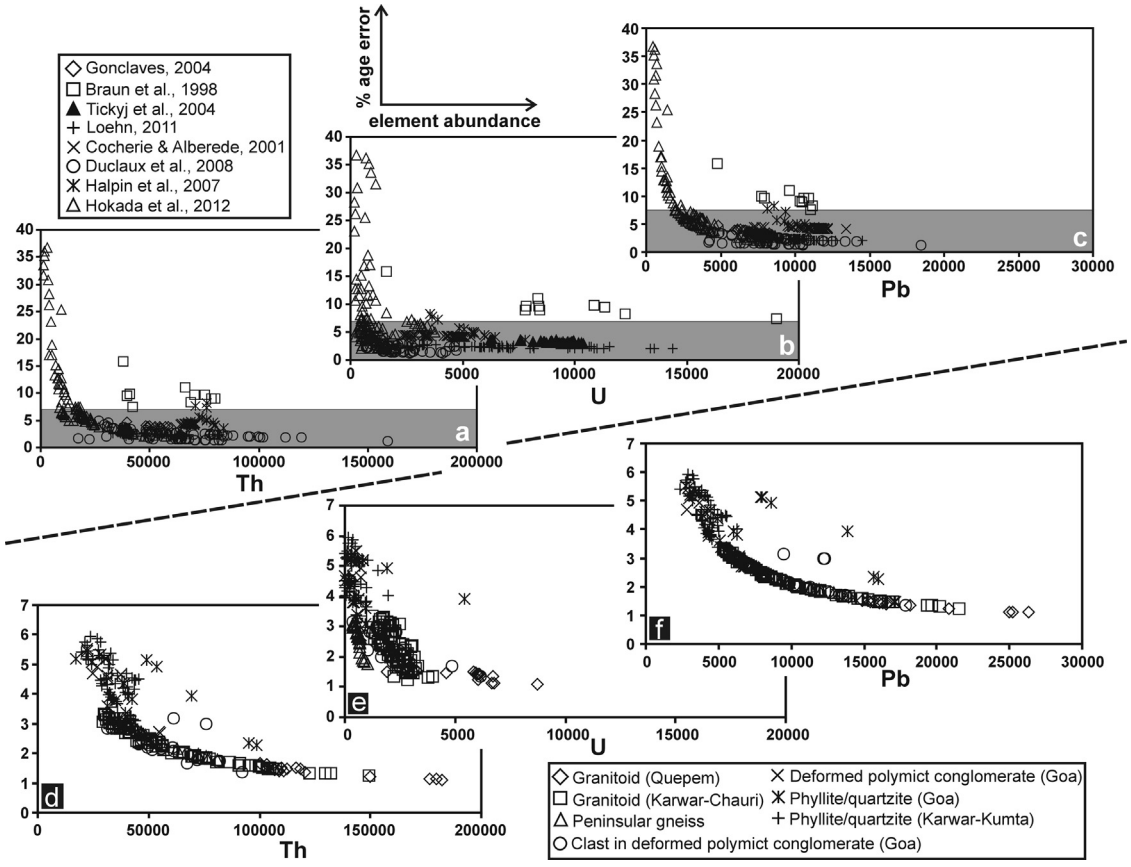

Fig. 11. Variations in % age error of chemically dated monazite spot ages against Th, U and Pb abundances (in ppm): (a–c) variations in spot age data (>2000 Ma) culled from literature (references in box, top left); (d–f) variations in spot age data (this study) obtained in different lithodemic units in WDC (box, bottom right) along the northern Konkan coast (Table 1, Data Repository[1]). Shaded areas in a–c demarcate the range of *X*- and *Y*-axes shown in d–f. For Hokada et al. (2012), the % age error is computed based on 1σ error in spot ages quoted by the authors.

5. Discussion

Smith and Giletti (1997) experimentally determined the closure temperature for diffusive Pb loss in monazites to be ~600 °C and 700 °C for cooling rates corresponding to 10 °C/Ma and 100 °C/Ma respectively. More recent estimation (Cherniak et al., 2004) suggests the closure temperature for Pb loss in monazite is significantly higher >900 °C for 10 °C/Ma cooling rate. Based on the available data, Pb loss in monazite may be considered to be arguably negligible at $T < 700$ °C (Cocherie et al., 1998; Copeland et al., 1988; Dahl, 1997; Mezger et al., 1991; Parrish, 1990; Spear and Parrish, 1996). Alternatively, monazites may grow by fluid-mediated dissolution-precipitation mechanisms over a wide range of metamorphic conditions (Finger et al., 1998; Grapes et al., 2005; Kim et al., 2009; Kohn and Malloy, 2004; Poitrasson et al., 1996), inclusive of growth at low-T (300–450 °C) corresponding to greenschist facies metamorphism (Cabella et al., 2001; Poitrasson et al., 2000; Rasmussen et al., 2005; Rasmussen and Muhling, 2009; Rekha et al., 2012) and hydrothermal alteration (Kempe et al., 2008; Rasmussen et al., 2006). At low-T condition, the detrital monazites are unstable and replaced by low-Th monazite, apatite, thorite and allanite (Rasmussen and Muhling, 2009).

5.1. Textural settings of monazites and significance of age determinations

In this section, the textural settings of monazites in Peninsular gneisses, para-schists/phyllites in the Karwar-Kumta and the Goa schist belts, deformed para-conglomerates in the Goa schist belt, and granitoid plutons in Karwar, Chauri and Quepem are discussed to understand the significance of EMP ages. In polygenetic monazites, geologically significant ages estimated from age populations of chemically distinct domains in texturally constrained monazites (Cocherie et al., 1998; Goncalves et al., 2004; Montel et al., 1996; Spear and Pyle, 2002; Williams et al., 2006), although chemically similar domains may also yield different ages, and vice versa (Williams et al., 1999). For the samples examined in this study, the methodology was applied to large-sized (80–500 μm long axis) monazites in granitoids and Peninsular gneisses, but for small-sized (typically < 10 μm) monazites with patchy, couple-of-microns wide chemical zones in low-grade metamorphic rocks of the supracrustal belts the exercise could not be implemented because radiation damage on the sample from exposure to electron beam was observed to be wider (3–4 μm diameter for ThO_2 abundance > 5 wt%) relative to the width of chemical zones. Thus the spot ages (Table 1) in the schists/phyllites correspond to monazite grain interiors, and multiple-ages in monazites were retrieved by statistical analysis of spot age data. In granitoids and gneisses, the radiation damage is wider (> 7–8 μm diameter) especially for higher-Th monazite (ThO_2 >10 wt%), but as the chemical zones in these monazites are wider than in the schist and phyllites, the chemically distinct domains in gneisses and granitoids could be accurately dated.

5.1.1. Peninsular gneiss

Monazites are rare in Peninsular gneisses. Monazites are circular to elliptical in shape, moderate to large-sized (diameter: 80–300 μm) and share stable boundaries with silicate phases. Monazites included in and located at grain/phase boundaries of

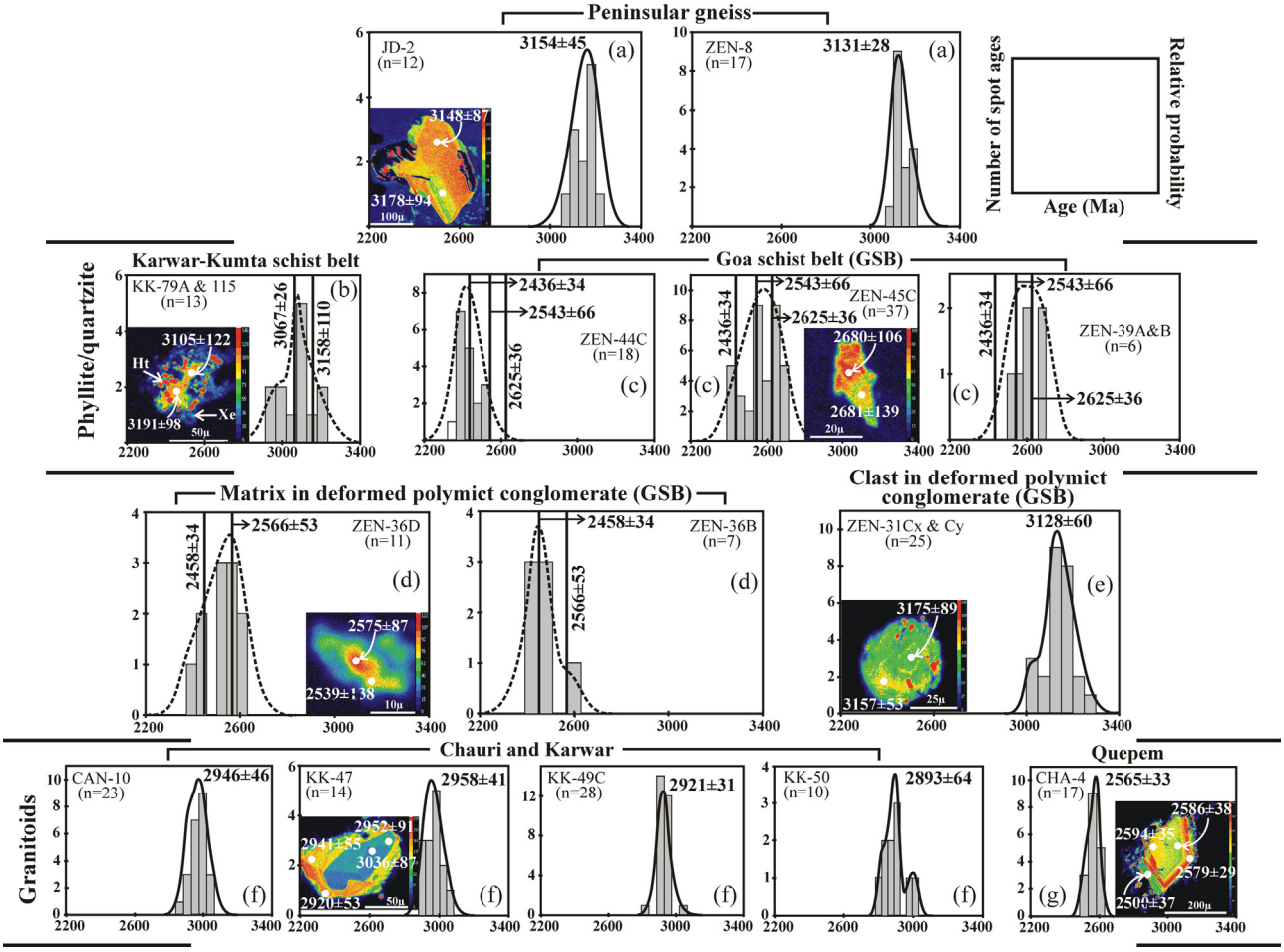

Fig. 12. Probability density and histogram plots (Isoplot/Ex; Ludwig, 2003) of monazite spot ages (data in Table 1) in (a) Peninsular gneiss (JD-2, ZEN-8), (b) phyllite/schist in the Karwar-Kumta schist belt (KK-79A, 115), (c) phyllite/schist in Goa schist belt (ZEN-44C, 45C, 39A, B), (d) foliated matrix in GSB deformed polymict conglomerate (ZEN-36B, D) (e) clasts in GSB polymict conglomerate (ZEN-31Cx, y), (f) Karwar and Chauri blastoporphyritic granitoids (CAN-10, KK-47, 49C and 50), and (g) Quepem granitoid (CHA-4). Spot age data in Table 1. For the Karwar-Kumta schist belt (b), the broken line (shown for visual aid) is the probability density plot if all spot ages were pooled into a single population. The vertical lines are the unmixed age components (Isoplot/Ex; Ludwig, 2003) from the same spot age data set. For the GSB phyllites and schists (c), the vertical lines are the statistically unmixed ages if all spot age data in the four samples are pooled together; the broken line is the probability density plot for data sets in individual samples (shown for visual aid). The vertical lines in foliated matrix in GSB polymict conglomerate (d) are the unmixed age components and the broken line is the probability density plot (shown for visual aid) for data sets in individual samples. In the remaining samples, the probability density plots are computed for the spot ages in each sample. '*n*' is the number of spot age analysis in each sample. The locations of the samples are in Fig. 4. X-ray Th maps of monazites with spot ages and 2σ errors keyed to the maps are provided as insets wherever relevant. (Th, U, Pb and Y X-ray maps for the grains are provided in Data Repository[2]). Monazite grain in phyllite (KK-115) is mantled by huttonite (Ht) and xenotime (Xe), Data Repository[2].

polygonized minerals are weakly zoned (Fig. 12a) or are chemically homogeneous (Fig. 13a and b). Ages in different zones in chemically zoned monazites (Fig. 12a) are within 2σ errors of spot ages. The large number of monazite spot ages in two samples JD-2 and ZEN-8 range between 3058 Ma and 3198 Ma (Table 1 and Fig. 12a). The age data pooled together constitute a single statistically significant population with the mean age 3138 ± 35 Ma. Given the coarse size of monazites, unlikely to have grown during low-T deformation-metamorphism, we infer the age to correspond with the age of anatectic amphibolite facies metamorphism (S_{1MG}/S_{2MG}) experienced by the migmatitic Peninsular gneisses.

5.1.2. *Phyllites, schists and quartzites*

In the Karwar-Kumta and the Goa schist belts, monazites are small (max length rarely > 10 μm), xenomorphic and appear chemically homogeneous in back-scattered electron images (Fig. 13c–e). In Th and Y maps, the small monazite grains exhibit unclear and fuzzy variations, but these zones are barely 1–2 μm wide and are difficult to analyze. Huttonite and xenotime aggregates replace strongly embayed margins of these monazites (Fig. 12b; Data Repository[2]). Monazites overgrowing tectonic fabrics in phyllites and schists are of metamorphic origin (Fig. 13c and e), however, monazite hosted in dynamically recrystallized quartz (Fig. 13d) could be detrital in origin or metamorphic in nature.

Chemical ages in monazites in the Karwar-Kumta schist belt (KK-79A, KK-115; Fig. 12b) and the Goa schist belt (ZEN-44C, 45C, 39A, B; Fig. 12c) belong to two distinct age groups. For the Karwar-Kumta schist belt, spot ages in KK-79A and 115 pooled together yield two unmixed age components, e.g. 3158 ± 110 Ma (84% of the age population) and 3067 ± 26 Ma (16% of the age population) (Fig. 12b). By contrast, the spot ages in ZEN-44C, 45C, 39A and 39B in the Goa schist belt pooled together yield three younger unmixed age clusters, 2436 ± 34 Ma (41% of the age population), 2543 ± 66 Ma (24% of the age population) and 2625 ± 36 Ma (35% of the age population) (Fig. 12c). The data demonstrates that metamorphism in the Goa schist belt is Neoarchean in age (temporally equivalent to the Chitradurga Group of the Dharwar Supergroup) in contrast to the Mesoarchean Karwar-Kumta schist belt (temporally equivalent to the Sargur Group). The chronological results are consistent with the inference made earlier that the Goa schist belt is structurally younger than the Karwar-Kumta schist belt.

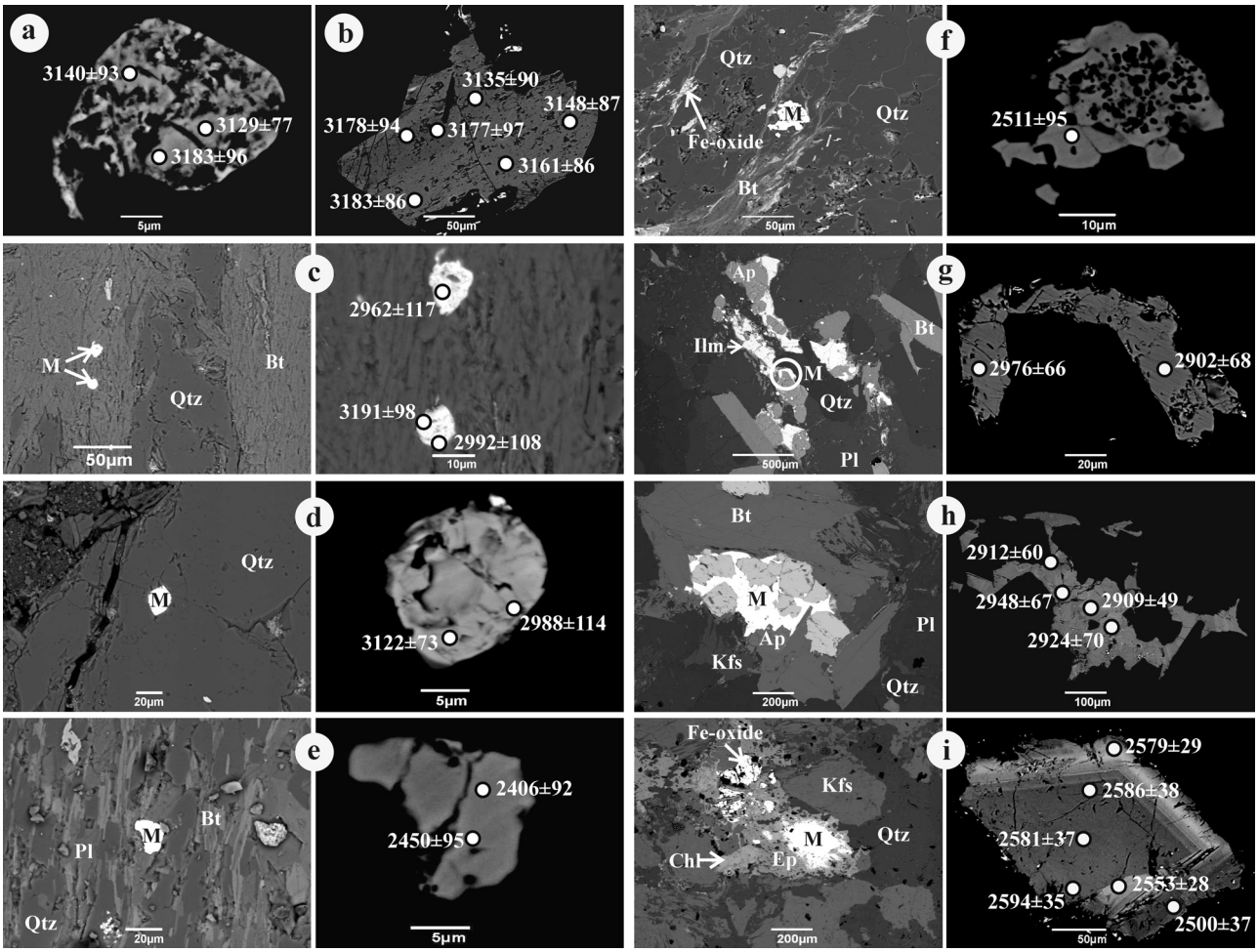

Fig. 13. BSE images of monazites (designated M) with textural settings, age, and 2σ error in Ma. (a, b) Sub-rounded to elliptical monazites in Peninsular gneiss. (c) Metamorphic monazites in M-domain overgrowing S_{3KK} foliation in the Karwar-Kumta schist belt. Note pre-S_{3KK} fabric in the inter folial Q-domains. (d) Monazite hosted within deformed quartz grain in quartzite from the Karwar-Kumta schist belt. Establishing if the monazite is detrital or metamorphic in origin is difficult. (e) Metamorphic monazite overgrowing S_{1GO} in the Goa schist belt defined by quartz ribbon and biotite aggregate. (f) Metamorphic monazite in meta-conglomerates from Goa schist belt overgrowing wispy S_{1GO} aggregates of phyllo-silicates. (g) A crescent-shaped monazite around lineated apatite in the Karwar blastoporphyritic granitoid. The apatite along with ilmenite and biotite define the earliest tectonic fabric in the foliated granitoid. (h) Skeletal monazite grown around Fe-oxide aggregate in blastoporphyritic granitoid. Note faint patchy zoning in monazite in BSE image (right). Age difference, if any, between different gray shades cannot be resolved within the errors of spot ages. (i) Monazite, with strong oscillatory zoning along margin, in aggregates of recrystallized quartz and K-feldspar is rimmed by epidote-chlorite corona in foliated Quepem granitoid. Within 2σ error of spot ages, age difference, if any, between the grain core and zoned margin cannot be resolved.

5.1.3. Para-conglomerates of the Goa schist belt

Monazites lodged within detrital clasts in para-conglomerates from the Goa schist belt are easily distinguished from metamorphic monazites overgrowing the fine-grained S_{1GO} chlorite-muscovite-biotite ± calcite fabric warping around clasts (Figs. 12d and 13f). Monazites hosted in tonalite clasts are older (mean age: 3128 ± 60 Ma; Fig. 12e) relative to prismatic monazite overgrowing the warping fabric with unmixed metamorphic age components, e.g. 2458 ± 34 Ma (40% of the age population) and 2566 ± 53 Ma (for the remaining age fraction) from two samples ZEN-36D and ZEN-36B (Fig. 12d). These ages retrieved from metamorphic monazites in the para-conglomerates ZEN-36B and ZEN-36D are similar to the ages of metamorphic monazites in the GSB schist/phyllite and quartzite. On the other hand, the range and mean age of clast-hosted monazites in the GSB para-conglomerates closely correspond to the ages retrieved from Peninsular gneisses, e.g. 3138 ± 35 Ma. This and the identical rare earth element patterns and abundances in monazites in the Peninsular gneiss clasts (Fig. 14a; Data Repository[1]) suggest the Peninsular gneisses were the source rocks for the Goa basin sediments. The gamut of monazite ages (Fig. 12e) in the GSB para-conglomerate ZEN-31Cx, y and phyllites/schists/quartzites (ZEN-44C, 45C, 39A and 39B) suggests the Goa basin formation post-dated 3.1–3.2 Ga deformation-metamorphism in the Peninsular gneisses and the Karwar-Kumta schist belt, but was older than 2.6 Ga when the basin probably closed.

5.1.4. Blastoporphyritic granitoids

Karwar-Chauri granitoids: Monazites occur in three textural settings. Round to sub-rounded and coarse (>100 μm, up to 500 μm) monazites occur in neo-crystallized quartz, quartz sub-grains, and at boundaries of polygonized quartz and feldspar. Monazites in polymineralic aggregates of Fe–Ti oxide, apatite and biotite defining the tectonic fabric are skeletal in shape and grow as mantles around apatite and Fe-oxides (Figs. 12f and 13g, h); rafts of apatite and Fe oxides are commonly included in these monazites. These monazites are clearly of metamorphic origin. In contrast to the chemically homogenous metamorphic monazites of the two textural types (Fig. 13g and h), monazites hosted in plagioclase porphyries are chemically zoned, with Th-poorer and Y-richer interiors relative to rim parts (Fig. 12f; Data Repository[2]). These large-sized monazites with chemically zoned rationally developed crystal faces appear to be of magmatic origin. The core to rim variations in ages in the zoned monazites are within the ±2σ error of

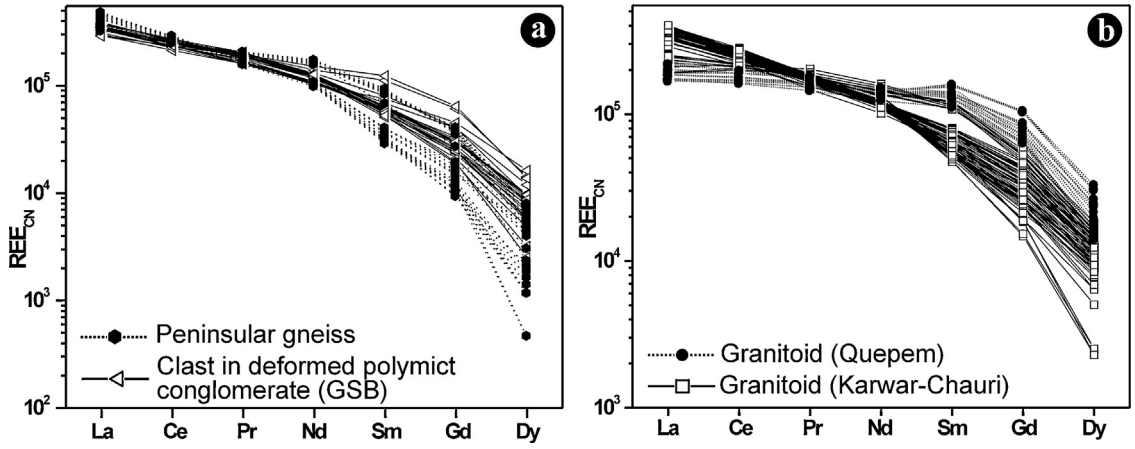

Fig. 14. Chondrite-normalized (Taylor and McClennan, 1985) REEs (La – Dy) plots of monazites: (a) Peninsular gneiss compared with Peninsular gneiss clasts in deformed polymict conglomerate (Goa schist belt); (b) Karwar-Chauri granitoid versus the Quepem granitoid.

spot ages (Fig. 12f), and age differences, if any, between magmatic (zoned) monazite and skeletal metamorphic monazite cannot be statistically resolved. The large number ($n = 75$; Fig. 12f) of spot ages in the Karwar-Chauri granitoid samples pooled together yield a statistically vetted single age population, 2924 ± 50 Ma. The age corresponds with low-T deformation-metamorphism of Karwar-Chauri granitoids that closely followed granitoid emplacement.

Quepem granitoid: Monazites in the Quepem granitoid pluton are coarse (60–300 μm in diameter) and euhedral in shape, and occur in recrystallized aggregates of quartz and K-feldspar. As with the Karwar-Chauri granitoid, monazites in Quepem granitoid are invariably zoned, with concentric chemically zoned rationally developed faces in monazites (Figs. 12g and 13i). The margins of these monazites are rimmed by epidote-allanite corona (Fig. 13i). Monazite in the Quepem granitoid shows rim ward increase in Th abundance; Y initially shows rim ward increase, and thereafter, decreases sharply near the margin (Fig. 12g; Data Repository[2]). Relative to monazites in the Karwar-Chauri granitoids, the Quepem granitoid is characterized by flatter and lower abundances of LREEs, while MREE and HREE abundances are somewhat higher (Fig. 14b; Data Repository[1]). The monazite spot ages in the Quepem granitoid vary from 2500 ± 37 to 2619 ± 37 Ma. The older ages retrieved from the coarse grains of zoned magmatic monazite possibly correspond to pluton emplacement, whereas the younger age cluster compares favorably with the mean age of metamorphism-deformation in the Goa schist belt. It appears that the Qupem granitoid ~500 Ma younger relative to the Karwar-Chauri granitoid plutons may have been causally related to deformation-metamorphism marking the closure of the Neoarchean Goa basin.

5.2. Correlating lithodemic units along the Konkan coast with WDC stratigraphic units

According to Swami Nath and Ramakrishnan (1981) and Ramakrishnan and Vaidyanadhan (2008), the Karwar-Kumta schists and the Goa schists belong to the Dharwar Supergroup (2.6–2.8 Ga); the Dharwar Supergroup in turn overlies the >3.0 Ga Peninsular gneiss that shares intrusive/tectonic contact with the Sargur Group (3.1–3.3 Ga). The monazite chemical age (3.1–3.2 Ga) and the sequence of fabric superposition of anatectic amphibolite-facies Peninsular gneisses along the Konkan coast are similar to those in the Peninsular gneisses reported elsewhere in the WDC (Naha et al., 1993; Taylor et al., 1984). The Karwar-Kumta schists of the Shimoga schist belt is correlated with the older Bababudan Group (2.6–2.8 Ga) of the Dharwar Supergroup by Swami Nath and Ramakrishnan (1981) and Ramakrishnan and Vaidyanadhan (2008). This is untenable based on the available data. The monazite chemical ages indicate that the greenschist facies Karwar-Kumta schists correlate with the 3.1–3.3 Ga Sargur Group rather than the Bababudan Group. The schists were tectonically accreted to the migmatitic gneisses (≈Peninsular gneiss). It stands to reason that the gneisses were not intrusive into the Karwar-Kumta schist (≈Sargur Group) as suggested by some workers (Swami Nath and Ramakrishnan, 1981; Ramakrishnan and Vaidyanadhan, 2008).

The existing U–Pb and Pb–Pb zircon ages and Rb–Sr and Pb–Pb whole-rock ages in the tonalite-granodiorite plutons, pods and dykes in the WDC lie between 2.9 and 3.1 Ga (Fig. 3). The range includes emplacement ages in well-studied intrusives at Halekote (3063 ± 39 Ma, Monrad, 1983; 3069 ± 28 Ma, Stroh et al., 1983), Chitradurga (2970 ± 100 Ma; Taylor et al., 1984) and Kuncha (3080 ± 76 Ma; Beckinsale et al., 1982). In comparison, the mean monazite chemical age (2924 ± 50 Ma) in the Karwar-Chauri granitoids is somewhat lower, e.g. by 100 Ma. The difference in age may suggest that the mean monazite age corresponds with the low-T deformation of the granitoids. But this appears unrealistic in view of the large sizes of the monazite grains hosted within weakly deformed plagioclase porphyries. Alternatively, felsic plutonism in the Mesoarchean may have been episodic as suggested by the field relations in Fig. 10, and the Karwar-Chauri granitoids possibly belong to a younger generation of felsic plutonism.

Recent studies by Hokada et al. (2012) constrain the deposition of supracrustal sequences of Lower Unit of the Chitradurga Group to be Late Neoarchean to Early Paleoproterozoic (2.3–2.5 Ga). We correlate the 2.3–2.7 Ga Goa schist belt to be coeval with Chitradurga Group. The 2.5–2.6 Ga Quepem granitoid in the Goa schist belt is in good agreement with available age data in granitoids from the Goa area, e.g. Rb–Sr whole rock age 2.65 ± 0.1 Ga (Chandranath/Quepem granodiorite-granite); 2.56 ± 0.09 Ga (Dudhsagar granite) and 2.65 ± 0.13 Ga (Londa granitoid) (Dhoundial et al., 1987) and from those in the inland areas in the WDC, e.g. Pb–Pb whole rock age 2.48 ± 0.08 Ga (meta-carbonate), 2.57 ± 0.03 Ga (meta-volcanics) from the Sandur schist belt (Russell et al., 1996) and Honnali area (Taylor et al., 1984) respectively, and SHRIMP U–Pb ages (2.52–2.59 Ga) obtained from zircon, titanite and xenotime-monazite in metamorphosed felsic volcanics, granite, and gold bearing pegmatites (Sarma et al., 2011). Similar dates (2.48 ± 0.07 Ga, 2.46 ± 0.14 Ga) are also obtained from dolomite-diopside-forsterite marble of the Sargur schists (Bettadabidu area) by Sarangi et al. (2007) using ID-TIMS ^{207}Pb–^{204}Pb in zircon. The age range (2.4–2.6 Ga) is attributed to tectonism related to E-W amalgamation of the East and the West Dharwar Cratons and the emplacement of syn-orogenic granitoids typified by the N-trending

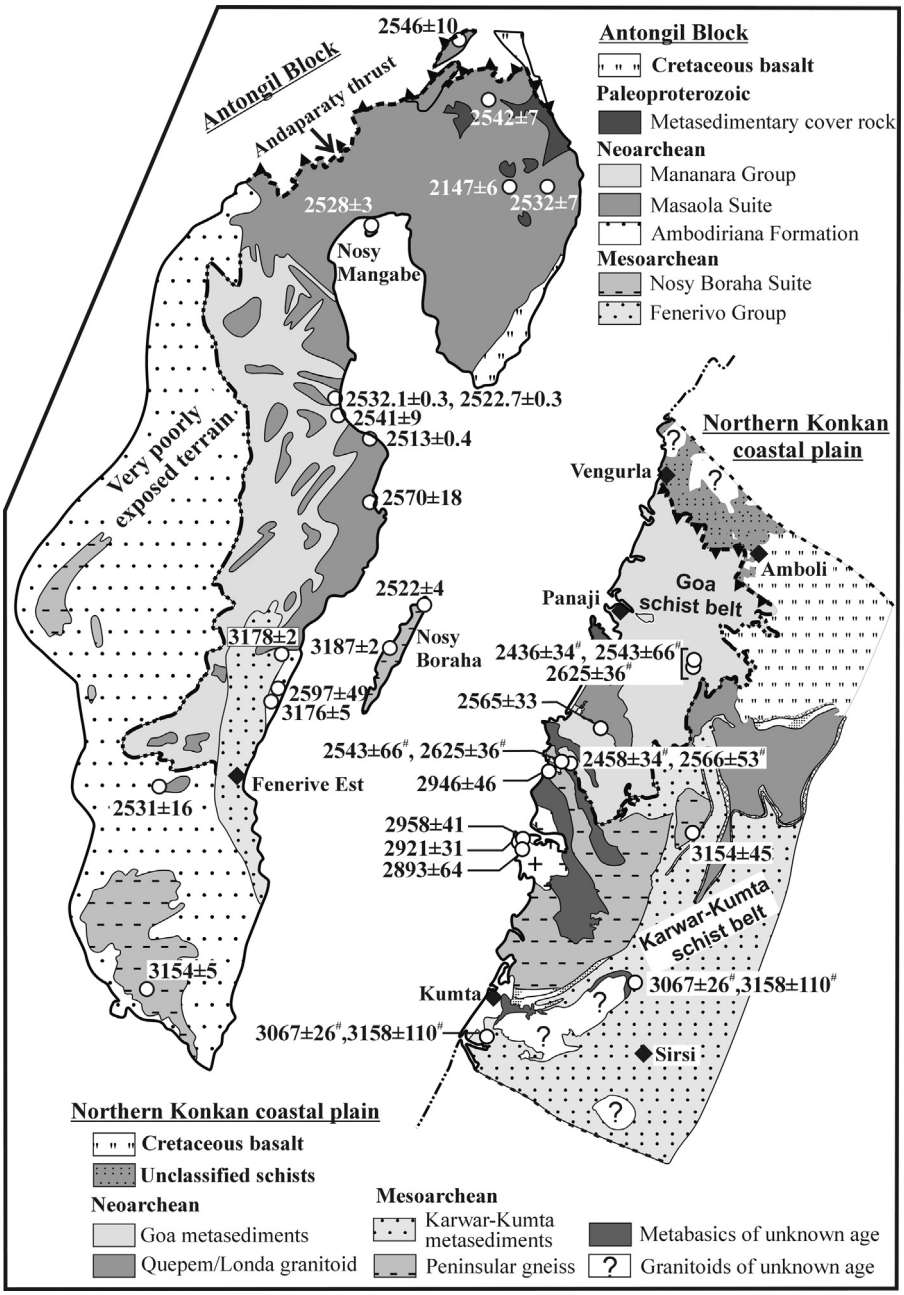

Fig. 15. A comparison between monazite ages from the northern Konkan coast (this study) and available age data from the Antongil Block (after Schofield et al., 2010). The extent of the Fenerivo Group is adopted from Tucker et al. (2011a). #Unmixed ages (refer Fig. 12).

Closepet pluton, e.g. ~2.5 Ga (Bhaskar Rao et al., 1992; Chadwick et al., 2000; Chardon and Jayananda, 2008; Friend and Nutman, 1991; Moyen et al., 2003; Peucat et al., 2007; Taylor et al., 1988). We infer that the ~2.57 Ga deformation-metamorphism and felsic plutonism that marked the closure of the Goa basin sediments formed broadly synchronous with the 2.4–2.6 Ga accretion of the West and the East Dharwar Cratons.

5.3. Brief outline of the geology of the Antongil-Masora Block, NE Madagascar

The northern Antongil Block, the southern Masora Block and the central Antananarivo Block constitute the Archean crustal domains along the northeastern coast of Madagascar (Schofield et al., 2010; Tucker et al., 2011a). The rock association, lithology and metamorphic grade vary greatly across the domain. The Antongil-Masora Blocks comprise three lithodemic units: (a) The Paleo/Mesoarchean (3.15–3.35 Ga) high-grade (migmatite) gneisses represented by the Nosy Boraha Suite and a group of stratified metasedimentary rocks (Fenerivo Group) which structurally overlies the Nosy Boraha Suite (Tucker et al., 1999, 2011a); (b) the expansive Neoarchean felsic intrusives (Collins et al., 2001, 2003; Paquette et al., 2003; Schofield et al., 2010; Tucker et al., 1999; Vachette and Hottin, 1970, 1979); and (c) the Neoarchean/Paleoproterozoic low-grade supracrustal of the Mananara Group (Raharimahefa and Kusky, 2006; Schofield et al., 2010) overlain by Cretaceous basalts. The Fenerivo Group in the central part (between Fenerivo and Soanierana-Ivongo) comprises extensively migmatized and polydeformed kyanite-fuchsite schist, garnet-amphibolite gneiss, quartzo-feldspathic schist, talc schist, and garnet-magnetite quartzite (Tucker et al., 2011a). Tucker et al. (2011a) reported $^{207}Pb/^{206}Pb$ zircon age of 3178 ± 2 Ma from feldspar-rich leucocratic gneiss within kyanite-muscovite

quartzo-feldspathic gneisses from the Fenerivo Group. These rocks were subjected to polyphase deformation, metamorphism, and partial melting at 2550 ± 42 Ma. The rocks in the Fenerivo Group are intruded by weakly foliated granitoids (2.55–2.51 Ga) of the Masoala Suite (Tucker et al., 2011a).

More than 90% of the exposed parts of the Antongil Block consists of Neoarchean rocks, out of which variably deformed granite, monzo-granite and granodiorite of the Masaola suite (Besairie, 1970) comprise ~30%. The rocks experienced weak low-grade (greenschist facies) deformation that post-dates the magmatic fabric (Schofield et al., 2010). U–Pb zircon ages in the Masoala Suite rocks yield tight age cluster of 2.49–2.57 Ga and rare 2.7 Ga (De Waele et al., 2008; Paquette et al., 2003; Schofield et al., 2010; Tucker et al., 1999). The Mananara Group includes low-grade (greenschist to epidote-amphibolite facies) metamorphic rocks (Collins, 2006; Schofield et al., 2010). The Ambodiriana Formation is characterized by rocks of distinctly higher metamorphic grade; e.g. locally interlayered migmatitic gneisses, staurolite-sillimanite-kyanite schists, foliated amphibolites, fuchsite quartzite and banded magnetite quartzites associated with ultramafic rocks (Schofield et al., 2010; Tucker et al., 2011a). The metasedimentary rocks from both the Mananara Group and the Ambodiriana Formation yield a tight age cluster of ~2.5 Ga (De Waele et al., 2008; Schofield et al., 2010). Schofield et al. (2010) reported an inherited age of 3176 ± 6 Ma and Pb-loss during 763 ± 13 Ma in supracrustal rocks from Ambodiriana Formation.

5.4. WDC – Antongil-Masora Block correlation

The existing ages of the lithodemic units in the Antongil-Masora Block, Madagascar and the monazite chemical ages obtained in this study in WDC lithologies along the Konkan coast are compared across the reconstructed coast line in Fig. 15. Early Cambrian-Neoproterozoic dates are not recorded in the monazite-dated rocks along the Konkan coast, unlike lithologies in the Antongil-Masora block that are demonstrably affected by Early Paleozoic tectonism (Collins, 2006; Raharimahefa and Kusky, 2006; Schofield et al., 2010). Due to the modifying effects of Neoproterozoic/Early Paleozoic tectonism, mesoscopic structures in the Peninsular gneisses in the WDC and the Antongil-Masora cannot be directly correlated. Nevertheless, in the Antongil Block, in domains along the coast and least modified by effects of Neoproterozoic/Early Paleozoic deformation, three folding events are identified in the Mesoarchean high-grade gneisses (Raharimahefa and Kusky, 2006). The first generation folds on gneissic layering with NE-trending axial planes are superposed by N-trending upright gently plunging second generation folds, and third generation folds with ENE-WSW trending axial plane (Raharimahefa and Kusky, 2006). These fold superposition structures correspond with the last three regional scale folding events identified in the low-grade phyllite/schist belts of the Karwar-Kumta and the Goa schist belts.

Along the western coast of India, the monazite ages decrease from Kumta (Mesoarchean) in the south (near) to Panaji (Paleoproterozoic/Neoarchean) in the north along the Konkan coast. Similar northward younging is also observed in the Antongil-Masora Block (Fig. 15). The Mesoarchean (~3.1 Ga) high-grade Peninsular gneisses of WDC are expansive along the Konkan coast, but their equivalents in NE Madagascar, e.g. the Nosy Boraha Suite, are exposed over limited extent in the Antongil-Masora Block (Fig. 15). At the other extreme of the age spectrum, metamorphic assemblages and monazite ages in the Goa schist/phyllite belt correlate well with rocks in the Mananara Group and the Ambodiriana Formation in Madagascar. The Late Neoarchean Quepem granitoid appears to correlate with the felsic plutonic Masoala Suite deformed at low temperature. But these Late Archean supracrustals and intrusives expansive in NE Madagascar are spatially restricted along the Konkan coast.

Based on chronological considerations, the lithological ensemble of kyanite-fuchsite schist, garnet-amphibolite gneiss, talc schist and garnet-magnetite quartzite (BIF) in the Fenerivo Group structurally overlying the Nosy Boraha Suite (Tucker et al., 1999, 2011a) appear to correlate well with the 3.1–3.3 Ga Sargur Group in WDC comprising fuchsite quartzite, forsterite-diopside marble, garnet-biotite schist, kyanite-staurolite ± corundum schist, chert, BIF, meta-komatiite and garnet-bearing amphibolite and ultramafic complex. Age-wise the ~3.1 Ga low-grade metamorphics in the Shimoga schist belt to which the Karwar-Kumta schists belong should also correlate with the Fenerivo Group in the Antongil-Masora Block. But it is unclear if low-grade schists are a conspicuous litho-unit in the Fenerivo Group. Considering available data, we tentatively correlate the Mesoarchean (~3.1 Ga) Fenerivo Group in the Anongil-Masora Block with the Sargur supracrustals vis-à-vis the Karwar-Kumta schists of the Shimoga schist belt in WDC. The ~2.9 Ga WDC granitoids are as yet unknown in the Anongil-Masora Block. The reason for this omission is unclear. Summarizing the available evidence suggests the Antongil Block and the WDC formed parts of a coherently evolved Mesoarchean to Neoarchean continental lithosphere that was part of the East Gondwana supercontinent prior to the assembly of East and West Gondwanaland. It appears that the Early Cambrian-Neoproterozoic tectonism associated with the Gondwana Supercontinent assembly did not affect the western coast of India or at least weakened considerably eastwards into India.

Acknowledgements

This work forms part of the doctoral dissertation of RS. RS acknowledges the financial support provided by CSIR-UGC research fellowship for the work. AB acknowledges the financial support through CPDA funds provided by the Institute for carrying out geological fieldwork in areas along the Konkan coast and the Western Ghats. The authors are thankful to S. Kumar (Department of Mathematics, IIT Kharagpur) for assisting with the statistical analysis of monazite age data. Magnolia (Department of Geology, Dhempe college of Arts and Science, Goa) and under-graduate students from the Department of Earth Sciences, Goa University showed us key outcrops for examination. The manuscript greatly benefited (scientifically and styling) from elaborate comments provided by R.D. Tucker, R.R. Parrish and two anonymous reviewers. We thank R.R. Parrish for his Editorial handling of the manuscript.

Appendix A. Supplementary data

Supplementary data associated with this article can be found, in the online version, at http://dx.doi.org/10.1016/j.precamres.2013.05.008.

References

Ancey, M., Bastenaire, F., Tixer, R., 1978. Application des methodes stastistiques en microanalyse. In: Maurice, F., Meny, L., Tixer, R. (Eds.), Microanalyse, microscopie electronique a balayage. Leś Editions du Physicien, Orsay, pp. 323–347.

Beckinsale, R.D., Drury, S.A., Holt, R.W., 1980. 3360 m-yr. old gneisses from the south Indian Craton. Nature 283, 469–470.

Beckinsale, R.D., Reeves-Smith, G., Gale, N.H., Holt, R.W., Thompson, B., 1982. Rb–Sr and Pb–Pb isochron ages and REE data for Archaean gneisses and granites, Karnataka state, South India. In: Ashwal, L.D. (Ed.), Indo-U.S. Workshop on the Precambrian of South India (abs.). NGRI, Hyderabad, pp. 35–36.

Berger, A., Stünitz, H., 1996. Deformation mechanisms and reaction of hornblende: examples from the Bergell tonalite (Central Alps). Tectonophysics 257, 149–174.

Besairie, H., 1970. Déscription géologique du massif ancien de Madagascar. In: Quatrième volume: la région centrale. 2. Le Système du Vohibory, Série schisto-quartzo-calcaire. Groupe d'Amborompotsy. Documentation du Bureau Géologique, Service Géologique de Madagascar, Tananarive, 177d, p. 86.

Bhaskar Rao, Y.J., Naha, K., Srinivasan, R., Gopalan, K., 1991. Geology, geochemistry and geochronology of the Archaean peninsular Gneiss around Gorur, Hassan District, Karnataka, India. Proceedings of the Indian Academy of Sciences (Earth and Planetary Sciences) 100, 399–441.

Bhaskar Rao, Y.J., Sivaraman, T.V., Pantulu, G.V.C., Gopalan, K., Naqvi, S.M., 1992. Rb–Sr ages of late Archaean metavolcanics and granites, Dharwar craton, South India and evidence for early Proterozoic thermotectonic events. Precambrian Research 59, 145–170.

Blasband, B., White, S.H., Brooijmans, P., Visser, W., De Boorder, H., 2000. Late Proterozoic extensional collapse in the Arabian-Nubian Shield. Journal of the Geological Society of London 157, 615–628.

Borg, S.G., De Paolo, D.J., 1991. Crustal structure and tectonics of the Antarctic margin of Gondwana and implications for the tectonic development of southeastern Australia. Tectonophysics 196, 339–358.

Braun, I., Montel, J.M., Nicollet, C., 1998. Electron microprobe dating of monazite from high-grade gneisses and pegmatites of the Kerala Khondalite Belt, southern India. Chemical Geology 146, 65–85.

Buchwaldt, R., Tucker, R.D., Dymek, R.F., 2003. Geothermobarometry and U–Pb geochronology of metapelitic granulites and pelitic migmatites from the Lokoho region, Northern Madagascar. American Mineralogist 88, 1753–1768.

Cabella, R., Lucchetti, G., Marescotti, P., 2001. Authigenic monazite and xenotime from pelitic metacherts in pumpellyite-actinolite-facies conditions, Sestri-Voltaggio zone, Central Liguria, Italy. Canadian Mineralogist 39, 717–727.

Cayley, R., 2011. Exotic crustal block accretion to the eastern Gondwanaland margin in the Late Cambrian Tasmania, the Selwyn Block, and implications for the Cambrian-Silurian evolution of the Ross, Delamerian, and Lachlan orogens. Gondwana Research 19, 628–649.

Chadwick, B., Vasudev, V.N., Hedge, G.V., 2000. The Dharwar craton, southern India, interpreted as the result of Late Archaean oblique convergence. Precambrian Research 99, 91–101.

Chardon, D., Jayananda, M., 2008. Three-dimensional field perspective on deformation, flow, and growth of the lower continental crust (Dharwar craton, India). Tectonics 27, TC1014.

Chatterjee, N., Nicolaysen, K., 2012. An intercontinental correlation of the mid-Neoproterozoic Eastern Indian tectonic zone: evidence from the gneissic clasts in Elan bank conglomerate, Kerguelen Plateau. Contributions to Mineralogy and Petrology 163, 789–806.

Cherniak, D.J., Watson, E.B., Grove, M., Harrison, T.M., 2004. Pb diffusion in monazite: a combined RBS/SIMS study. Geochimica et Cosmochimica Acta 68, 829–840.

Cocherie, A., Albarede, F., 2001. An improved U–Th–Pb age calculation for electron microprobe dating of monazite. Geochimica et Cosmochimica Acta 65, 4509–4522.

Cocherie, A., Legendre, O., Peucat, J.J., Kouamelan, A., 1998. Geochronology of polygenic monazites constrained by in situ electron microprobe Th–U–total Pb determination: implications for Pb behaviour in monazite. Geochimica et Cosmochimica Acta 62, 2475–2497.

Collins, A.S., 2006. Madagascar and the amalgamation of Central Gondwana. Gondwana Research 9, 3–16.

Collins, A.S., Fitzsimons, I.C.W., Kinny, P.D., Brewer, T.S., Windley, B.F., Kröner, A., Razakamanana, T., 2001. The Archaean rocks of Central Madagascar: their place in Gondwana. In: Cassidy, K.F., Dunphy, J.M., Van Kranendonk, M.J. (Eds.), 4th International Archaean Symposium 2001. Extended Abstracts. AGSO–Geoscience Australia, Record 2001/37, pp. 294–296.

Collins, A.S., Kröner, A., Fitzsimons, C.W., Razakamanana, T., 2003. Detrital footprint of the Mozambique ocean: U–Pb SHRIMP and Pb evaporation zircon geochronology of metasedimentary gneisses in eastern Madagascar. Tectonophysics 375, 77–99.

Collins, A.S., Pisarevsky, S.A., 2005. Amalgamating eastern Gondwana: the evolution of the Circum-Indian Orogens. Earth Science Reviews 71, 229–270.

Copeland, P., Parrish, R.R., Harrison, T.M., 1988. Identification of inherited radiogenic Pb in monazite and its implications for U–Pb systematics. Nature 333, 760–763.

Crowley, J.L., Chatterjee, N., Bowring, S.A., Sylvester, P.J., Myers, J.S., Searle, M.P., 2005. U–(Th)–Pb dating of monazite and xenotime by EMPA, LA-ICPMS, and IDTIMS: examples from the Yilgarn Craton and Himalayas. In: 15th Annual Goldschmidt Conference Abstract, p. A19.

Dahl, P.S., 1997. A crystal-chemical basis for Pb retention and fission track annealing systematics in U-bearing minerals, with implications for geochronology. Earth and Planetary Science Letters 150, 277–290.

Dalziel, I.W.D., 1991. Pacific margins of Laurentia and East Antarctica-Australia as a conjugate rift pair: evidence and implications for an Eocambrian supercontinent. Geology 19, 598–601.

De Waele, B., Thomas, R.J., Schofield, D.I.S., Bauer, W., Walsh, G.J., Lidke, D., Goodenough, K.M., Key, R.M., Rabarimanana, M.H., Rafahatelo, J.M., Ralison, A.V., Randramananjara, T., 2008. An overview of the Archaean Antongil Block, northern Madagascar. In: 33rd IGC, Oslo.

De Wit, M.J., 2003. Madagascar: heads it's a continent, tails it's an island. Annual Reviews of Earth and Planetary Sciences 31, 213–248.

Dhoundial, D.P., Sarkar, D.K., Trivedi, J.R., Gopalan, K., Potts, P.J., 1987. Geochronology and geochemistry of Precambrian granitic rocks of Goa, southwest India. Precambrian Research 36, 287–302.

Duclaux, G., Rolland, Y., Ruffet, G., 2008. Superimposed Neoarchaean and Paleoproterozoic tectonics in the Terre Adelie Craton (East Antarctica): evidence from Th–U–Pb ages on monazite and $^{40}Ar/^{39}Ar$ ages. Precambrian Research 167, 316–338.

Finger, F., Broska, I.B., Roberts, M.P., Schermaier, A., 1998. Replacement of primary monazite by apatite-allanite-epidote coronas in an amphibolite facies granite gneiss from the eastern Alps. American Mineralogist 83, 248–258.

Fitzsimons, I.C.W., 2000. A review of tectonic events in the East Antarctic Shield and their implications for Gondwana and earlier supercontinents. Journal of African Earth Sciences 31, 3–23.

French, J.E., Heaman, L.M., 2010. Precise U–Pb dating of Paleoproterozoic mafic dyke swarms of the Dharwar craton, India: implications for the existence of the Neoarchean supercraton Sclavia. Precambrian Research 183, 416–441.

French, J.E., Heaman, L.M., Chacko, T., Rivard, B., 2004. Global mafic magmatism and continental break up at 2.2 Ga: evidence from the Dharwar craton India. Geological Society of America Abstracts with Programs 36 (5), 340 (Denver Annual Meeting, November 7–10, 2004).

Friend, C.R.L., Nutman, A.P., 1991. Shrimp U–Pb Geochronology of the Closepet Granite and Peninsular Gneiss, Karnataka, South-India. Journal of the Geological Society of India 38, 357–368.

Goncalves, P., Nicollet, C., Montel, J.-M., 2004. Petrology and in situ U–Th–Pb monazite geochronology of ultrahigh-temperature metamorphism from the Andriamena Mafic Unit, North–Central Madagascar. Significance of a Petrographical P–T path in a polymetamorphic context. Journal of Petrology 45, 1923–1957.

Grapes, R., Bucher, K., Hoskin, P.W.O., 2005. Monazite-epidote reaction in amphibolite grade blackwall rocks. European Journal of Mineralogy 17, 553–566.

Gurnis, M., 1988. Large-scale mantle convection and the aggregation and dispersal of supercontinents. Nature 332, 695–699.

Hacker, B.R., Christie, J.M., 1991. Observational evidence for a possible new diffusion path. Science 25 l, 67–70.

Halls, H.C., Kumar, A., Srinivasan, R., Hamilton, M.A., 2007. Paleomagnetism and U–Pb geochronology of eastern trending dykes in the Dharwar craton India: feldspar clouding, radiating dyke swarms and position of India at 2.37 Ga. Precambrian Research 155, 47–68.

Halpin, J.A., White, R.W., Clarke, G.L., Kelsey, D.E., 2007. The Proterozoic P–T-t evolution of the Kemp Land Coast, East Antarctica: constraints from Si-saturated and Si-undersaturated metapelites. Journal of Petrology 48, 1321–1349.

Hoffman, P.F., 1991. Did the breakout of Laurentia turn Gondwanaland inside-out? Science 252, 1409–1412.

Hokada, T., Horie, K., Satish-Kumar, M., Ueno, Y., Nasheeth, A., Mishima, K., Shiraishi, K., 2012. An appraisal of Archaean supracrustal sequences in Chitradurga Schist Belt, Western Dharwar Craton, Southern India. Precambrian Research, http://dx.doi.org/10.1016/j.precamres.2012.04.006.

Jayananda, M., Kano, T., Peucat, J.J., Channabasappa, S., 2008. 3.35 Ga komatiite volcanism in the western Dharwar craton southern India: constraints from Nd isotopes and whole-rock geochemistry. Precambrian Research 162, 160–179.

Jercinovic, M.J., Williams, M.L., 2005. Analytical perils (and progress) in electron microprobe trace element analysis applied to geochronology: back-ground acquisition, interferences, and beam irradiation effects. American Mineralogist 90, 526–546.

Jöns, N., Emmel, B., Schenk, V., Razakamanana, T., 2009. From orogenesis to passive margin-the cooling history of the Bemarivo Belt (N Madagascar), a multi-thermo chronometer approach. Gondwana Research 16, 72–81.

Katz, M.B., Premoli, C., 1979. India and Madagascar in Gondwanaland based on matching Precambrian lineaments. Nature 279, 312–315.

Kempe, U., Lehmann, B., Wolf, D., Rodionov, N., Bombach, K., Schwengfelder, U., Dietrich, A., 2008. U–Pb SHRIMP geochronology of Th-poor, hydrothermal monazite: an example from the Llallagua tin-porphyry deposit, Bolivia. Geochimica et Cosmochimica Acta 72, 4352–4366.

Kim, Y., Yi, K., Cho, M., 2009. Parageneses and Th–U distributions among allanite, monazite, and xenotime in Barrovian-type metapelites, Imjingang belt, central Korea. American Mineralogist 94, 430–438.

Kohn, M.J., Malloy, M.A., 2004. Formation of monazite via prograde metamorphic reactions among common silicates: implications for age determinations. Geochimica et Cosmochimica Acta 68, 101–113.

Kretz, R., 1983. Symbols for rock-forming minerals. American Mineralogist 68, 277–279.

Kröner, A., Hegner, E., Collins, A.S., Windley, B.F., Brewer, T.S., Razakamanana, T., Pidgeon, R.T., 2000. Age and magmatic history of the Antanarivo Block, central Madagascar, as derived from zircon geochronology and Nd isotopic systematics. American Journal of Science 300, 251–288.

Kumar, A., Bhaskar Rao, Y.J., Sivaraman, T.V., Gopalan, K., 1996. Sm–Nd ages of Archean metavolcanics of the Dharwar craton, South India. Precambrian Research 80, 205–216.

Kusky, T.M., Matsah, M.I., 2003. Neoproterozoic dextral faulting on the Najd Fault System, Saudi Arabia, preceded sinistral faulting and escape tectonics related to closure of the Mozambique Ocean. Geological Society of London, 327–361, Special Publications 206.

Lafrance, B., Vernon, R.H., 1999. Coupled mass transfer and microfracturing in gabbroic mylonites. In: Snoke, A.W., Tullis, J.A., Todd, V.R. (Eds.), Fault-Related Rocks: A Photographic Atlas. Princeton University Press, New Jersey, pp. 204–207.

Lawver, L.A., Scotese, C.R., 1987. A revised reconstruction of Gondwanaland. In: McKenzie, G.W. (Ed.), Gondwana Six: Structure, Tectonics and Geophysics. American Geophysical Union, Washington, DC, pp. 17–23.

Loehn, C.W., 2011. Investigation of the monazite chemical dating technique. Virginia Polytechnic Institute and State University, pp. 85, http://scholar.lib.vt.edu/theses/available/etd-05122011-164811/unrestricted/LoehnPhDETD.pdf (Unpublished Ph.D. thesis).

Ludwig, K.R., 2003. User's Manual for ISOPLOT/3.00: A Geochronological Toolkit for Microsoft Excel, Berkeley Geochron Centre Special Publication 4, pp. 71.
Mahan, K.H., Goncalves, P., Williams, M.L., Jercinovic, M.J., 2006. Dating metamorphic reactions and fluid flow: application to exhumation of high-P granulites in a crustal-scale shear zone, western Canadian Shield. Journal of Metamorphic Geology 24, 193–217.
Maya, J.M., Bhutani, R., Balakrishnan, S., 2011. $^{146,147}Sm$–$^{142,143}Nd$ studies of komatiites from Western Dharwar Craton, India: Implications for depleted mantle evolution in Early Archean. In: Abstract, Goldschmidt Conference, August 14–19, 2011.
McWilliams, M.O., 1981. Paleomagnetism and Precambrian tectonic evolution of Gondwana. In: Kröner, A. (Ed.), Precambrian Plate Tectonics. Elsevier, Amsterdam, pp. 649–687.
Meen, J.K., Rogers, J.J.W., Fullagar, P.D., 1992. Lead isotopic compositions of the Western Dharwar Craton, southern India: evidence for distinct Middle Archean terranes in a Late Archean craton. Geochimica et Cosmochimica Acta 56, 2455–2470.
Meert, J.G., Van der Voo, R., Ayub, S., 1995. Paleomagnetic investigation of the Late Proterozoic Gagwe lavas and Mbozi complex, Tanzania and the assembly of Gondwana. Precambrian Research 69, 113–131.
Merlet, C., 1992. Quantitative electron probe microanalysis: new accurate $\phi(\rho z)$ description. Microchimica Acta 12, 107–115.
Mezger, K., Rawnsley, C.M., Bohlen, S.R., Hanson, G.N., 1991. U–Pb garnet, sphene, monazite and rutile ages: implications for the duration of high-grade metamorphism and cooling histories, Adirondack Mts, New York. Journal of Geology 99, 415–428.
Monrad, J.R., 1983. Evolution of sialic terranes in the vicinity of Holenarasipur belt, Hassan district, Karnataka, India. Geological Society of India Memoir 4, 343–365.
Montel, J.M., Foret, S., Veschambre, M., Nicollet, C., Provost, A., 1996. Electron microprobe dating of monazite. Chemical Geology 131, 37–53.
Moores, E.M., 1991. Southwest U.S.-East Antarctic (SWEAT) connection: a hypothesis. Geology 19, 425–428.
Moyen, J.F., Martin, H., Jayananda, M., Auvray, B., 2003. Late Archaean granites: a typology based on the Dharwar Craton (India). Precambrian Research 127, 103–123.
Mukhopadhyay, D., 1986. Structural patterns in the Dharwar craton. Journal of Geology 94, 167–186.
Naha, K., Chatterjee, A.K., 1982. Axial plane folding in the Bababudan hill ranges of Karnataka. Indian Journal of Earth Sciences 9, 37–43.
Naha, K., Mukhopadhyay, D., Dastidar, S., Mukhopadhyay, R.P., 1995. Basement-cover relations between a granite gneiss body and its metasedimentary envelope: a structural study from the Early Precambrian Dharwar tectonic province, southern India. Precambrian Research 72, 283–299.
Naha, K., Srinivasan, R., Gopalan, K., Pantulu, G.V.C., Subba Rao, M.V., Vrevsky, A.B., Bogomolov, Y.E.S., 1993. The nature of the basement in the Archaean Dharwar craton of southern India and the age of the Peninsular Gneiss. Proceedings of the Indian Academy of Sciences (Earth and Planetary Sciences) 102, 547–556.
Naha, K., Srinivasan, R., Jayaram, S., 1990. Structural evolution of the Peninsular Gneiss – an early Precambrian migmatitic complex from South India. Geologische Rundschau 79, 99–109.
Naha, K., Srinivasan, R., Jayaram, S., 1991. Sedimentational, structural, and migmatitic history of the Archean Dharwar tectonic province, southern India. Proceedings of the Indian Academy of Sciences (Earth and Planetary Sciences) 100, 413–433.
Naha, K., Srinivasan, R., Mukhopadhyay, D., 1996. Structural studies and their bearing on the Early Precambrian history of the Dharwar tectonic province, southern India. Proceedings of the Indian Academy of Sciences (Earth and Planetary Sciences) 105, 379–412.
Naha, K., Srinivasan, R., Naqvi, S.M., 1986. Structural unity in the early Precambrian Dharwar tectonic province Peninsular India. Quarterly Journal of the Geological, Mining and Metallurgical Society of India 58, 219–243.
Narayanaswami, S., 1966. Tectonics of the Cuddapah Basin. Journal of the Geological Society of India 7, 33–50.
Nutman, A.P., Chadwick, B., Ramakrishnan, M., Viswanatha, M.N., 1992. SHRIMP U–Pb ages of detrital zircon in Sargur supracrustal rocks in western Karnataka, southern India. Journal of the Geological Society of India 39, 367–374.
Paquette, J.L., Moine, B., Rakotondrazafy, M.A.F., 2003. ID-TIMS using the stepwise dissolution technique versus ion microprobe U–Pb dating of metamict Archean zircons from NE Madagascar. Precambrian Research 121, 73–84.
Parrish, R.R., 1990. U–Pb dating of monazite and its application to geological problems. Canadian Journal of Earth Sciences 27, 1431–1450.
Payne, J.L., Hand, M., Barovich, K.M., Reid, A., Evans, D.A.D., 2009. Correlations and reconstruction models for the 2500–1500 Ma evolution of the Mawson continent. In: Reddy, S.M., et, al. (Eds.), Palaeoproterozoic Supercontinents and Global Evolution, Geological Society of London Special Publication 323, pp. 319–355.
Peucat, J.J., Bouhallier, H., Fanning, C.M., Jayananda, M., 1995. Age of the Holenarsipur Greenstone-Belt: relationships with the surrounding gneisses (Karnataka, South India). Journal of Geology 103, 701–710.
Peucat, J.J., Mahabaleswar, B., Jayananda, M., 2007. Age of younger tonalitic magmatism and granulitic metamorphism in the South Indian transition zone (Krishnagiri area); comparison with older Peninsular gneisses from the Gorur–Hassan area. Journal of Metamorphic Geology 11, 879–888.
Pili, E., Ricard, Y., Lardeaux, J.-M., Sheppard, S.M.F., 1997. Lithospheric shear zones and mantle-crust connections. Tectonophysics 280, 15–29.
Poitrasson, F., Chenery, S., Bland, D.J., 1996. Contrasted monazite hydrothermal alteration mechanisms and their geochemical implications. Earth and Planetary Science Letters 145, 79–96.
Poitrasson, F., Chenery, S., Shepherd, T.J., 2000. Electron microprobe and LA-ICP-MS study of monazite hydrothermal alteration: implications for U–Th–Pb geochronology and nuclear ceramics. Geochimica et Cosmochimica Acta 64, 3283–3297.
Prabhakar, N., 2013. Resolving poly-metamorphic Paleoarchean ages by chemical dating of monazites using multi-spectrometer U, Pb and Th analyses and sub-counting methodology. Chemical Geology (in press).
Radhakrishna, T., Balasubramanian, G., Mathew, J., Krishnendu, N.R., 2004. Mantle processes and geodynamics: Inferences from mafic dykes of south India. In: Ravindra Kumar, G.R., Subhash, N. (Eds.), Earth System Science and Natural Resource Management. Silver Jubilee Compendium, pp. 3–25.
Raharimahefa, T., Kusky, T.M., 2006. Structural and remote sensing studies of the southern Betsimisaraka Suture, Madagascar. Gondwana Research 10, 186–197.
Raharimahefa, T., Kusky, T.M., 2010. Temporal evolution of the Angavo and related shear zones in Gondwana: constraints from LA-MC-ICP-MS U–Pb zircon ages of granitoids and gneiss from central Madagascar. Precambrian Research 182, 30–42.
Ramakrishnan, M., Vaidyanadhan, R., 2008. Geology of India. Publications of the Geological Society of India, Bangalore 1, 556p.
Rasmussen, B., Fletcher, I.R., Sheppard, S., 2005. Isotopic dating of the migration of a low-grade metamorphic front during orogenesis. Geology 33, 773–776.
Rasmussen, B., Muhling, J.R., 2009. Reactions destroying detrital monazite in greenschist-facies sandstones from the Witwatersrand basin, South Africa. Chemical Geology 264, 311–327.
Rasmussen, B., Sheppard, S., Fletcher, I.R., 2006. Testing ore deposit models using in situ U–Pb geochronology of hydrothermal monazite: Paleoproterozoic gold mineralization in northern Australia. Geology 34, 77–80.
Rekha, S., Bhattacharya, A., Viswanath, T.A., 2012. Microporosity linked fluid focusing and monazite instability in greenschist facies para-conglomerates, western India. Geochimica et Cosmochimica Acta 105, 187–205.
Rogers, J.J.W., Santosh, M., 2003. Supercontinents in Earth history. Gondwana Research 6, 357–368.
Russell, J., Chadwick, B., Krishna Rao, B., Vasudev, V.N., 1996. Whole-rock Pb/Pb isotopic ages of Late Archaean limestones, Karnataka, India. Precambrian Research 78, 261–272.
Sacks, P.E., Nambiar, C.G., Walters, L.J., 1997. Dextral Pan-African shear along the south western edge of the Achanakovil shear belt, South India: constraints of Gondwana reconstruction. Journal of Geology 105, 275–284.
Sarangi, S., Gopalan, K., Srinivasan, R., 2007. Small scale sampling for Pb–Pb dating of marbles: example from the Sargur supracrustal rocks, Dharwar Craton, South India. Precambrian Research 152, 83–91.
Sarma, D.S., Fletcher, I.R., Rasmussen, B., McNaughton, N.J., Ram Mohan, M., Groves, D.I., 2011. Archaean gold mineralization synchronous with late cratonization of the Western Dharwar Craton India: 2.52 Ga U–Pb ages of hydrothermal monazite and xenotime in gold deposits. Mineralium Deposita 46, 273–288.
Scherrer, N.C., Engi, M., Gnos, E., Jakob, V., Liechti, A., 2000. Monazite analysis; from sample preparation to microprobe age dating and REE quantification. Schweizer Mineralogische und Petrographische Mitteilungen 80, 93–105.
Schofield, D.I., Thomas, R.J., Goodenough, K.M., De Waele, B., Pitfield, P.E.J., Key, R.M., Bauer, W., Walsh, G., Lidke, D., Ralison, A.V., Rabarimanana, M., Rafahatelo, J.M., Randriamananjara, T., 2010. Geological evolution of the Antongil Craton, NE Madagascar. Precambrian Research 182, 187–203.
Shackleton, R.M., 1996. Precambrian collision tectonics in Africa. In: Coward, M.P., Ries, A.C. (Eds.), Collision tectonics: Geological Society of London. Special Publication 76, pp. 345–362.
Simpson, C., 1985. Deformation of granitic rocks across the ductile-brittle transition. Journal of Structural Geology 7, 503–511.
Smith, H.A., Giletti, B.J., 1997. Lead diffusion in monazite. Geochimica et Cosmochimica Acta 61, 1047–1055.
Sommer, H., Kröner, A., Hauzenberger, C., Muhongo, S., Wingate, M.T.D., 2003. Metamorphic petrology and zircon geochronology of high-grade rocks from the central Mozambique Belt of Tanzania: crustal recycling of Archean and Palaeoproterozoic material during the Pan-African orogeny. Journal of Metamorphic Geology 21, 915–934.
Spear, F.S., Parrish, R., 1996. Petrology and petrologic cooling rates of the Valhalla Complex, British Columbia, Canada. Journal of Petrology 37, 733–765.
Spear, F.S., Pyle, J.M., 2002. Apatite, monazite, and Xenotime in metamorphic rocks. Reviews in Mineralogy and Geochemistry 48, 293–331.
Spear, F.S., Pyle, J.M., Cherniak, D., 2009. Limitations of chemical dating of monazite. Chemical Geology 266, 218–230.
Stern, R.J., 1994. Arc assembly and continental collision in the Neoproterozoic East Africa Orogen: implications for the consolidation of Gondwanaland. Annual Review of Earth and Planetary Sciences 22, 319–351.
Stroh, P.T., Marwad, J.R., Fullagar, P.O., Naqvil, S.M., Hussain, S.M., Rogers, J.J.W., 1983. 3000 My old Halekote trondhjemite: a record of stabilisation of the Dharwar craton. Geological Society of India Memoir 4, 365–376.
Swami Nath, J., Ramakrishnan, M., 1981. Early Precambrian supracrustals of Southern Karnataka. Geological Survey of India Memoir 112, 351.
Taylor, P.N., Chadwick, B., Friend, C.R.L., Ramakrishnan, M., Moorbath, S., Viswanatha, M.N., 1988. New age data on the geological evolution of southern India. Journal of the Geological Society of India 31, 155–157.
Taylor, P.N., Chadwick, B., Moorbath, S., Ramakrishnan, M., Viswanatha, M.N., 1984. Petrography, chemistry and isotopic ages of Peninsular Gneiss, Dharwar acid

volcanic rocks and the Chitradurga granite with special reference to the late Archaean evolution of the Karnataka craton. Precambrian Research 23, 349–375.

Taylor, S.R., McClennan, S.M., 1985. The Continental Crust: Its Composition and Evolution. Blackwell, Oxford, pp. 312.

Thomas, R.J., De Waele, B., Schofield, D.I., Goodenough, K.M., Horstwood, M., Tucker, R.D., Bauer, W., Annells, R.A., Howard, K.B., Walsh, G., Rabarimanana, M., Rafahatelo, J.M., Ralison, A.V., Randriamananjara, T., 2009. Geological evolution of the Neoproterozoic Bemarivo Belt, northern Madagascar. Precambrian Research 172, 279–300.

Tickyj, H., Hartmann, L.A., Vasconcellos, M.A.Z., Philipp, R.P., Remus, M.V.D., 2004. Electron microprobe dating of monazite substantiates ages of major geological events in the southern Brazilian shield. Journal of South American Earth Sciences 16, 699–713.

Torsvik, T.H., Smethurst, M.A., Meert, J.G., Van der Voo, R., McKerrow, W.S., Sturt, B.A., Brasier, M.D., Walderhaug, H.J., 1996. Continental breakup and collision in the Neoproterozoic and Paleozoic – a tale of Baltica and Laurentia. Earth Science Reviews 40, 229–258.

Trompette, R., 2000. Gondwana evolution: its assembly around 600 Ma. Comptes Rendus de l'Academie des Sciences, Serries IIA. Earth and Planetary Science Letters 330, 305–315.

Tucker, R.D., Ashwal, L.D., Handke, M.J., Hamilton, M.A., Le Grange, M., Rambeloson, R.A., 1999. U–Pb geochronology and isotope geochemistry of the Archean and Proterozoic rocks of north-central Madagascar. Journal of Geology 107, 135–153.

Tucker, R.D., Roig, J.Y., Delor, C., Amelin, Y., Goncalves, P., Rabarimanana, M.H., Ralison, A.V., Belcher, R.W., 2011a. Neoproterozoic extension in the Greater Dharwar Craton: a reevaluation of the Betsimisaraka suture in Madagascar. Canadian Journal of Earth Sciences 48, 389–417.

Tucker, R.D., Roig, J.Y., Macey, P.H., Delor, C., Amelin, Y., Armstrong, R.A., Rabarimanana, M.H., Ralison, A.V., 2011b. A new geological framework for south central Madagascar, and its relevance to the out-of-Africa hypothesis. Precambrian Research 185, 109–130.

Unrug, R. (Ed.), 1996. Geodynamic Map of Gondwana Supercontinent Assembly, Scale 1:10 Million. Bureau de Recherches Geologiques et Minieres, Orleans, France.

Vachette, M., Hottin, G., 1970. Age au strontium des granites d'Antongil et del'Androna (Nord-Est et Centre-Nord de Madagascar). In: Comptes Rendus Semaine Géologie de Madagascar, pp. 73–76.

Vachette, M., Hottin, G., 1979. The Precambrian of Madagascar through whole-rock Rb/Sr isochron data. Histoire du Gondwana vue de Madagascar, Antananarivo.

Veevers, J.J., 2004. Gondwanaland from 650–500 Ma assembly through 320 Ma merger in Pangea to 185–100 Ma breakup: supercontinental tectonics via stratigraphy and radiometric dating. Earth-Science Reviews 68, 1–132.

Vlach, S.R.F., 2010. Th–U–Pb_T Dating by Electron Probe Microanalysis, Part I. Monazite. Analytical Procedures and Data Treatment. Geol. USP, Sér. cient. 10, 61–85.

Weil, A.B., Van der Voo, R., MacNiocall, C., Meert, J.G., 1998. The Proterozoic supercontinent Rodinia: paleomagnetically derived reconstructions for 1100–800 Ma. Earth and Planetary Science Letters 154, 13–24.

Williams, M.L., Jercinovic, M.J., Terry, M.P., 1999. Age mapping and dating of monazite on the electron microprobe: deconvoluting multistage tectonic histories. Geology 27, 1026.

Williams, M.L., Jercinovic, M.J., Goncalves, P., Mahan, K., 2006. Format and philosophy for collecting, compiling, and reporting microprobe monazite ages. Chemical Geology 225, 1–15.

Williams, M.L., Jercinovic, M.J., Hetherington, C.J., 2007. Microprobe monazite geochronology: understanding geologic processes by integrating composition and chronology. Annual Review in Earth and Planetary Sciences 35, 137–175.

Wilson, J.T., 1966. Did the Atlantic close and then re-open? Nature 211, 676–681.

Windley, B.F., Razafiniparany, A., Razakamanana, T., Ackermand, D., 1994. Tectonic framework of the Precambrian of Madagascar and its Gondwana connections: a review and reappraisal. Geologisches Rundschau 83, 642–659.

Yoshida, M., Santosh, M., 1996. Southernmost Indian peninsula and the Gondwanaland. In: Santosh, M., Yoshida, M. (Eds.), The Archaean and Proterozoic terrains of southern India within East Gondwana, 3. Gondwana Research Group, Memoir, pp. 15–24.